Second-generation operational algorithm: Retrieval of aerosol properties over land from inversion of Moderate Resolution Imaging Spectroradiometer spectral reflectance

Robert C. Levy,[1,2,3] Lorraine A. Remer,[2] Shana Mattoo,[1,2] Eric F. Vermote,[4] and Yoram J. Kaufman[2]

Received 20 July 2006; revised 23 January 2007; accepted 26 February 2007; published 13 July 2007.

[1] Since first light in early 2000, operational global quantitative retrievals of aerosol properties over land have been made from Moderate Resolution Imaging Spectroradiometer (MODIS) observed spectral reflectance. These products have been continuously evaluated and validated, and opportunities for improvements have been noted. We have replaced the surface reflectance assumptions, the set of aerosol model optical properties, and the aerosol lookup table (LUT). This second-generation operational algorithm performs a simultaneous inversion of two visible (0.47 and 0.66 μm) and one shortwave-IR (2.12 μm) channel, making use of the coarse aerosol information content contained in the 2.12 μm channel. Inversion of the three channels yields three nearly independent parameters, the aerosol optical depth (τ) at 0.55 μm, the nondust or fine weighting (η), and the surface reflectance at 2.12 μm. Retrievals of small-magnitude negative τ values (down to -0.05) are considered valid, thus balancing the statistics of τ in near zero τ conditions. Preliminary validation of this algorithm shows much improved retrievals of τ, where the MODIS/Aerosol Robotic Network τ (at 0.55 μm) regression has an equation of: y = 1.01x + 0.03, R = 0.90. Global mean τ for the test bed is reduced from $\sim$0.28 to $\sim$0.21.

Citation: Levy, R. C., L. A. Remer, S. Mattoo, E. F. Vermote, and Y. J. Kaufman (2007), Second-generation operational algorithm: Retrieval of aerosol properties over land from inversion of Moderate Resolution Imaging Spectroradiometer spectral reflectance, *J. Geophys. Res.*, *112*, D13211, doi:10.1029/2006JD007811.

1. Introduction

[2] Aerosols are major players in Earth's climate, radiation budget, and cloud processes, and increasingly sophisticated and accurate remote sensing techniques have been introduced to characterize aerosols and their effects. Especially for aerosols over land, the first operational global satellite dataset has been provided by the Moderate Resolution Imaging Spectroradiometer (MODIS). Since MODIS' launch aboard *Terra* (in late 1999) and aboard *Aqua* (in early 2002), the use of the MODIS aerosol products has grown exponentially. Since launch, MODIS data and specifically aerosol data have been used to answer scientific questions about radiation and climate [e.g., *Intergovernmental Panel on Climate Change*, 2001; *Yu et al.*, 2006]. MODIS data are also being used for applications not previously considered, such as monitoring of surface air quality [e.g., *Chu et al.*, 2003; *Al-Saadi et al.*, 2005].

[3] The MODIS instruments aboard Terra and Aqua both measure spectral radiance in 36 channels, in resolutions between 250 m and 1 km (at nadir). In polar orbit, approximately 700 km above the Earth, MODIS views a swath $\sim$2300 km, resulting in near daily global coverage of Earth's land/ocean/atmosphere system. The swath is broken into 5-min "granules," each $\sim$2030 km long. The operational algorithm over land uses MODIS reflectance data in three channels (0.47, 0.66, and 2.12 μm; bands 3, 1, and 7) to retrieve total spectral (function of wavelength, λ) "aerosol optical depth" (AOD or τ_λ) and "fine aerosol weighting" (FW or η). Additional channels are used to perform cloud masking and other decisions for pixel selection. The primary products (including τ and η) are reported at 10 km resolution (at nadir), at λ = 0.55 μm.

[4] *Kaufman et al.* [1997a] introduced the strategy for retrieving aerosol over land from MODIS. The top of the atmosphere reflectance ρ^* at a particular wavelength λ can be approximated by

$$\rho^*_\lambda(\theta_0,\theta,\phi) = \rho^a_\lambda(\theta_0,\theta,\phi) + \frac{F_\lambda(\theta_0)T_\lambda(\theta)\rho^s_\lambda(\theta_0,\theta,\phi)}{1 - s_\lambda\rho^s_\lambda(\theta_0,\theta,\phi)} \quad (1)$$

[1]Science Systems and Applications Inc., Lanham, Maryland, USA.
[2]Laboratory for Atmospheres, NASA Goddard Space Flight Center, Greenbelt, Maryland, USA.
[3]Department of Atmospheric and Oceanic Science, University of Maryland, College Park, Maryland, USA.
[4]Department of Geography, University of Maryland, College Park, Maryland, USA.

Copyright 2007 by the American Geophysical Union.
0148-0227/07/2006JD007811

where ρ^a_λ is the atmospheric "path reflectance," $F_{d\lambda}$ is the "normalized downward flux" for zero surface reflectance, T_λ represents "upward total transmission" into the satellite field of view, s_λ is the "atmospheric backscattering ratio," and ρ^s_λ is the angular "surface reflectance." These are in turn functions of solar zenith angle, satellite zenith angle, and solar/satellite relative azimuth angles (θ_0, θ, and φ, respectively). Except for the surface reflectance, each term on the right-hand side of equation (1) is a function of the Rayleigh scattering, aerosol type, and aerosol loading (τ). While equation (1) is technically valid for a uniform, Lambertian surface, the bidirectional properties of the surface reflectance can be approximated by the value of the surface reflectance for the relevant solar and satellite viewing geometry [*Kaufman et al.*, 1997a]. Assuming that a small set of aerosol types and loadings can describe the range of global aerosol, the algorithm relies on a lookup table (LUT) that contains precomputed simulations of these aerosol conditions. The goal of the algorithm is to examine the LUT to determine the conditions that best mimic the MODIS-observed spectral reflectance $\rho^m{}_\lambda$, and retrieve the associated aerosol properties (including τ and η). The difficulty lies in making the most appropriate assumptions about both the surface and atmospheric contributions.

[5] Since launch, the aerosol products have been monitored for quality, so the algorithm has been continuously improved and updated for bug fixes, cloud masking, and pixel selection. Updates to the operational algorithm are known as "versions," whereas products from particular processing periods are grouped into "collections." Details of a previous version (V4.2.2) and the products of "Collection 004" (C004) were described by *Remer et al.* [2005]. The second-generation algorithm described here and in the "Algorithm Theoretical Basis Document for Collection 5" (ATBD-2006; found online at http://modis-atmos.gsfc.nasa.gov/MOD04_L2/index.html), is known operationally as "V5.2" and is used for generated Collection 5 (C005) products. All updates to the operational algorithm can be found online at: http://modis-atmos.gsfc.nasa.gov/MOD04_L2/history.

[6] In order to justify the use of MODIS aerosol products for any application, the uncertainty of the retrieval must be quantified. Prior to launch, sensitivity tests and airborne simulations suggested that MODIS should be able to retrieve τ to within 20–30% (the expected error) over most vegetated and semivegetated land surfaces [e.g., *Kaufman et al.*, 1997a]. Since launch, validation studies suggested the expected error over land could be represented by

$$\Delta\tau = \pm 0.05 \pm 0.15\tau \tag{2}$$

[*Remer et al.*, 2005]. To this end, a number of papers attempted to "validate" the retrieved properties of C004 and before by comparing MODIS derived values to standard (ground truth) aerosol measurements, using the colocation method of *Ichoku et al.* [2002]. Ground-based Sun photometers, especially from the Aerosol Robotic Network (AERONET [*Holben et al.*, 1998]), have provided the bulk of the comparison data [e.g., *Chu et al.*, 2002; *Levy et al.*, 2005; *Remer et al.*, 2005]. Most of these validation studies have shown that although MODIS generally derived τ to within the expected error, MODIS tended to overestimate τ for small τ and underestimate for high τ [*Chu et al.*, 2002; *Remer et al.*, 2005; *Levy et al.*, 2005]. At 0.55 μm, we can consider a representative MODIS/AERONET regression of $\tau_{0.55}$ over land as

$$\tau_{\mathrm{MODIS}} = 0.1 + 0.9\,\tau_{\mathrm{AERONET}}. \tag{3}$$

[7] Any aerosol retrieval algorithm must make many assumptions about the complicated satellite signal. As a result of systematically evaluating key assumptions contained in the C004 algorithm family, we developed the second generation of operational MODIS retrieval over land (for processing C005). Section 2 introduces relevant C004 MODIS products and AERONET data used for development. Section 3 summarizes the aerosol optical models and the new LUT (described in a separate paper [*Levy et al.*, 2007]). Derivation of surface reflectance properties are discussed in section 4. Section 5 introduces a new retrieval methodology, and section 6 discusses the C005 products. Finally, we show provisional validation of the new algorithm in section 7.

2. MODIS C004 and AERONET L2A Data Sets

[8] For this work, we made extensive use of both MODIS and AERONET data products. Aerosol products have been derived from Terra reflectance observations since 2000 and since 2002 from Aqua. As of early 2005, most MODIS observations of colocated.calibrated reflectance ("Level 1B") through 2004 had been processed or reprocessed into "Level 2" products (L2) using consistent retrieval algorithms, creating the set of products known collectively as C004.

[9] The Sun photometers of AERONET provide a comprehensive data set of aerosol properties. These include direct "Sun" measurements of spectral τ in four or more wavelengths (to include 0.44, 0.67, 0.87, and 1.02 μm), and indirect "sky" measurements that lead to retrievals of aerosol optical properties and aerosol size distributions [*Holben et al.*, 1998]. These data go through rigorous calibration and cloud screening processes. The AERONET direct Sun measurements are made approximately every 15 min during midday and more often during sunrise and sunset. In addition to spectral τ, AERONET also provides estimates of columnar water vapor w (precipitable water in units of centimeters). *O'Neill et al.* [2003] developed a method for retreiving η from the direct Sun measurements of spectral τ. The AERONET sky radiance measurements are made less often (about once per hour), and are inverted simultaneously either assuming spherical aerosol particles [*Dubovik and King*, 2000] and/or spheroid particles [*Dubovik et al.*, 2002; *Dubovik et al.*, 2006]. The choice of spheres or spheroids depends on the quality of the sky radiance fitting. Under either particle assumption, the fundamental derived parameters include spectral τ_λ, spectral complex refractive index, the volume size distribution as a function of 22 radius size bins (dV/dlnR), and fitting error to the radiance measurements. Additional parameters are then calculated, that include Ångstrom exponents, properties of bimodal lognormal (fine and coarse mode) aerosol distributions, spectral single scattering albedo (*SSA* or ω_0), and asymmetry parameter (g) of the lognormal modes.

[10] At some sites, AERONET has been reporting since 1993, and as of early 2005, most of the AERONET data have been reprocessed and quality assured by the AERONET team. These products are also known as "Level 2," but to differentiate them from the MODIS products, we denote the AERONET products as "L2A."

[11] Although the actual products provided by MODIS and AERONET are not necessarily physically identical, in many cases they are comparable. For example, by fitting a quadratic equation through the logarithms of τ and wavelength, AERONET τ can be interpolated to 0.55 μm [*Eck et al.*, 1999] to match directly with the MODIS retrieval. Comparison of η is trickier. Over land, MODIS considers η to be the contribution of the fine-dominated model (the nondust model) to the total τ, the AERONET sky retrievals designate η to be the volume contribution from aerosol smaller than radius of 0.6 μm, whereas the O'Neill method separates fine and coarse aerosol by spectral behavior. Practically, however, the definitions of μ are similar enough so that they should be correlated [*Kleidman et al.*, 2005; *Anderson et al.*, 2006; *Chu et al.*, 2005].

[12] Over 15,000 pairs of MODIS and AERONET "Sun" data, at over 200 global sites, have been colocated in time via the technique of *Ichoku et al.* [2002]. A valid MODIS/AERONET match is considered when there at least five (out of a possible 25) MODIS retrievals (10 km $\times$ 10 km resolution) within the box, and at least two (out of a possible five) AERONET observations within the hour. The colocation retrieves the spatial average of MODIS and the temporal average of AERONET, as well as the values of the nearest pixel and temporal scan. This colocated data set was used for a number of applications described in this document, including evaluation of surface reflectance parameterization, and validation of MODIS products.

3. Aerosol Models and LUT

3.1. Aerosol Models and Optical Properties

[13] A number of studies [e.g., *Chu et al.*, 2002; *Remer et al.*, 2005; *Levy et al.*, 2005] demonstrated that comparison of C004 (and previous) MODIS products over land, against AERONET Sun retrievals, leads to regression of τ having slope less than one. This means that MODIS tends to underestimate optical depth, especially as the optical depth increases. *Ichoku et al.* [2002] and *Levy et al.* [2005] found that updating the assumed aerosol properties in Southern Africa and the U.S. mid-Atlantic improved the retrieval in each of these regions, respectively. These results suggested that the MODIS algorithm should consider revising the aerosol optical models that represent the global variability of aerosol optical properties. AERONET sky retrievals of size distribution and optical properties present a globally representative, long-term, and independent optical measure of aerosol properties for deriving new models.

[14] Details of the derivation and resulting aerosol models are described in separate manuscripts (*Levy et al.* [2007] and ATBD-2006), but we summarize them here. We began with nearly 14,000 AERONET sky retrievals (both spherical and spheroid assumptions) satisfying AERONET team recommended $\tau_{0.44} > 0.4$, (τ measured at 0.44 μm). Retrievals using assumed spheres generally described sites dominated by fine (radius < 0.6 μm) aerosols, whereas retrievals using assumed spheroids generally represented sites dominated by coarse (radius > 0.6 μm) aerosols. Performing cluster analysis upon the spherical retrievals, by retrieved ω_0 and g, resulted in three aerosol types that represent the global fine-dominated aerosol regimes. The averaged aerosol properties for each cluster were assumed to represent a unique aerosol type. These include a "nonabsorbing" aerosol model ($\omega_0 \sim 0.95$), presumably corresponding to urban/industrial aerosol in the industrialized northern hemisphere, an "absorbing" ($\omega_0 \sim 0.85$) aerosol model found in the known sooty and/or savanna-burning regions of South America and Africa, and a "moderately absorbing" aerosol model representative of biomass burning and incomplete fossil fuel burning in the developing world. Similar cluster analysis of spheroid retrievals showed that a single model represented global dust aerosol. Each aerosol "model" is comprised of two lognormal modes, either dominated by the fine mode (the three spherical models) or the coarse mode (the spheroid model).

[15] The average aerosol properties of each type were fed into a Mie code or T-matrix code (depending on spherical or spheroid assumptions), that were integrated over size distribution, to result in calculations of scattering/extinction properties. From these properties, the spectral dependence of τ and phase functions were characterized and summarized in tables (*Levy et al.* [2007]; ATBD-2006). These aerosol models were compared with the aerosol models utilized within the C004 algorithm and with the well-known "Continental" model.

[16] On the basis of the dominant aerosol type found during clustering, an aerosol type was "assigned" to each AERONET site (as a function of season) and then extrapolated to include the surrounding region. These regions were mapped onto a 1° longitude $\times$ 1° latitude grid, such that a fine aerosol type is assigned for each grid point, globally. As more information becomes available, it should be easy to update this map.

3.2. C005 Lookup Table

3.2.1. Radiative Transfer Code

[17] The C004 (and previous) LUTs were calculated using "SPD," the scalar version of the RT code written by *Dave* [1970], a code that is a standard in the remote sensing community. However, *Fraser et al.* [1989] suggested and *Levy et al.* [2004] demonstrated that under some geometries, neglecting polarization would lead to significant errors in top of atmosphere reflectance, further leading to significant errors (>10% or >0.1) in τ retrieval. Dave also provided a vector (polarized) option to the code (VPD), although it was not well maintained within the MODIS community. Therefore we desired a vector code that is well understood and suitable for creating the LUT, that in scalar mode, our choice of RT code should be consistent with the Dave benchmark. Also, it should reasonably match the *Ahmad and Fraser* [1982] calculations used for the over ocean aerosol retrieval [*Remer et al.*, 2005]. *Levy et al.* [2004] employed RT3, the polarized radiative transfer model of *Evans and Stephens* [1991]. This plane-parallel adding/doubling code allows for polarization to be turned on or off, by changing only one line within an input file. Thus it was easy to compare the results to

Table 1. Characteristics of MODIS Channels Used in the Aerosol Retrieval

Band	Bandwidth, μm	Weighted Central Wavelength, μm	Resolution, m	Rayleigh Optical Depth
1	0.620–0.670	0.646	250	0.0520
2	0.841–0.876	0.855	250	0.0165
3	0.459–0.479	0.466	500	0.1948
4	0.545–0.565	0.553	500	0.0963
5	1.230–1.250	1.243	500	0.0037
6	1.628–1.652	1.632	500	0.0012
7	2.105–2.155	2.119	500	0.0004

the Dave code's scalar mode and then upgrade to vector mode to include polarization effects. Under most geometries and optical depths, differences between the two RT codes are less than 0.001 (which is about 1%).

[18] As noted by *Levy et al.* [2007], the aerosol scattering phase function elements and extinction efficiencies (that are inputs to RT3) are calculated by integrating (over size distribution) the results of either the Mie code (MIEV [*Wiscombe*, 1981]) or the T-matrix kernel code [*Dubovik et al.*, 2002, 2006] depending on spherical or spheroid assumptions. Assuming a Rayleigh atmosphere and realistic layering of the aerosol, the Legendre moments of the combined Rayleigh/aerosol are computed for each layer of a U.S. Standard Atmosphere [*U.S. Government Printing Office*, 1976]. These moments are fed into RT3 to calculate TOA reflectance and total fluxes.

3.2.2. MODIS Channel Center Wavelengths and Rayleigh Optical Depth

[19] The MODIS 0.47 μm blue band (channel 3) stretches between 0.459 and 0.479 μm (http://modis.gsfc.nasa.gov). The sea-level Rayleigh optical depth (*ROD* or τ_R) drops drastically over this channel, from about 0.203 at 0.459 μm to 0.170 at 0.479 μm [*Bodhaine et al.*, 1999]. The choice of "center" wavelength to model and its associated ROD is crucial to obtaining unbiased aerosol retrieval. This is also an issue for the red 0.66 μm channel (channel 1: 0.620–0.670 μm), but since the RODs are only about one-quarter as in the blue, the decision is much less crucial. In C004, the assumed ROD was 0.186 for channel 3 and 0.048 for channel 1. The 6S RT code [*Vermote et al.*, 1997] models the MODIS channel filter functions and suggests that the ROD values should be more like 0.193 and 0.051, respectively, for the two channels. The MODIS aerosol over ocean algorithm [*Tanré et al.*, 1997; *Ahmad and Fraser*, 1982] assumes the RODs for the channels as 0.195 and 0.052, respectively.

[20] For C005, reevaluation of the MODIS channel filter functions showed that central wavelengths for channels 3 and 1 are 0.466 and 0.644 μm, respectively. According to *Bodhaine et al.* [1999], associated sea level ROD values are 0.194 and 0.052, respectively, which leads to consistency with the aerosol over ocean algorithm. Similar calculations for the 0.55 and 2.12 μm channels (channels 4 and 7) suggest center wavelengths of 0.553 and 2.119 μm and RODs of 0.092 and 0.0004, respectively. Note that although the center wavelengths are known, we will continue to designate MODIS channels 3, 4, 1, and 7 as the 0.47, 0.55, 0.66, and 2.12 μm channels for brevity and consistency with common usage. Table 1 lists the MODIS aerosol channels, along with the Rayleigh optical depth assumed for the band.

3.2.3. Description of the LUT

[21] As we will expand upon later, the second generation algorithm over land performs a simultaneous inversion of three channels (0.47, 0.66, and 2.12 μm) to retrieve τ, η, and the surface reflectance (e.g., *Levy et al.* [2007]; ATBD-2006). The inversion technique requires that the LUT be "indexed" like as for the over-ocean algorithm [*Tanré et al.*, 1997; *Remer et al.*, 2005]. Since the principal product is τ at 0.55 μm, the LUT is indexed in relation to this channel. In support of the C005 algorithm, the LUT is computed at the four central wavelengths (0.466, 0.553, 0.644, and 2.119 μm) representing the MODIS channels 3, 4, 1, and 7. The aerosol model-dependent parameters of equation (1) are calculated for several values of aerosol total loadings (indexed by τ at 0.55 μm), and for a variety of geometry. Each of the spherical aerosol models (Continental, moderately absorbing, absorbing, and nonabsorbing) and the one spheroid model (dust) should be represented within the LUT.

[22] The scattering and reflectance parameters are calculated for seven aerosol loadings ($\tau_{0.55}$ = 0.0, 0.25, 0.5, 1.0, 2.0, 3.0, and 5.0). TOA reflectance is calculated for nine solar zenith angles (θ_0 = 0.0, 6.0, 12.0, 24.0, 36.0, 48.0, 54.0, 60.0, and 66.0), 16 sensor zenith angles (θ = 0.0 to 65.8, approximate increments of 6.0, based on Lobatto quadrature with eight abscissa points (e.g., http://mathworld.wolfram.com/LobattoQuadrature.html)), and 16 relative azimuth angles (φ = 0.0 to 180.0 increments of 12.0). All of these parameters are calculated assuming a surface reflectance of zero. These are similar to the indices and geometry calculated for C004 LUT.

[23] When surface reflectance is present, the second term in equation (1) is nonzero. The flux is a function only of the atmosphere, however, the atmospheric backscattering term, s, and the transmission term, T, are functions of both the atmosphere and the surface. Therefore RT3 is run two additional times with distinct positive values of surface reflectance.

$$s = \left(1/\rho_1^s\right)\left(1 - \left(F_d T \rho_1^s / \left(\rho^* - \rho^a\right)\right)\right) \quad \text{and} \quad s = \left(1/\rho_2^s\right)\left(1 - \left(F_d T \rho_2^s / \left(\rho^* - \rho^a\right)\right)\right) \tag{4}$$

Here, we chose values of 0.1 and 0.25 for our surface reflectance. $\rho^s{}_1$ and $\rho^s{}_2$. These two equations can be solved for the two unknowns, s and T. These values of F_d, s, and T are included within the LUT, for each τ index, wavelength, and aerosol model.

4. VISvs2.12 Surface Reflectance Assumptions

[24] When performing atmospheric retrievals from MODIS or any other satellite, the major challenge is separating the total observed reflectance into atmospheric and surface contributions (e.g., equation (1)) and then defining the aerosol contribution. Over the open ocean,

the surface reflectance is nearly zero in the 0.66 μm and longer wavelength channels, so assuming negligible surface reflectance in these channels is a good approximation. Moving from coastline onto land, however, the surface reflectance in 0.66 μm and longer channels can be far from zero and vary over surface type. As the land surface and the atmospheric signals are comparable, errors of 0.01 in assumed surface reflectance can lead to errors on the order of 0.1 in τ retrieval [*Kaufman et al.*, 1997b]. Errors in multiple wavelengths can lead to poor retrievals of spectral τ, which in turn would be useless for estimating size parameters.

[25] *Kaufman et al.* [1997b] observed that over vegetated and dark soiled surfaces, the surface reflectance in some visible (VIS) wavelengths correlated with the surface reflectance at 2.12 μm, and in fact, were nearly fixed ratios of that in the 2.12 μm channel. Parallel simulations by vegetation canopy models showed that the physical reason for the correlation was the combination of absorption of visible light by chlorophyll and infrared radiation by liquid water in healthy vegetation [*Kaufman et al.*, 2002]. As applied in the C004 algorithm, surface reflectance at 0.47 μm and 0.66 μm were assumed to be one-quarter and one-half, respectively, of the surface reflectance at 2.12 μm. We note these relationships as the "0.47vs2.12" and "0.66vs2.12" ratios and collectively as the "VISvs2.12" ratios.

[26] Yet regression of C004 (and prior) MODIS-derived τ to AERONET Sun photometer data [*Chu et al.*, 2002; *Remer et al.*, 2005] showed that while the products generally agreed ($\sim$60–65%) to within the expected errors of equation (2), there was a positive offset of about 0.1 (equation (3)). Since C004 generally overestimated τ in pristine conditions, the assumed boundary conditions, including assumptions of surface reflectance, must be questioned. From data observed during the Chesapeake Lighthouse and Aircraft Measurements for Satellites (CLAMS) experiment of 2001, *Levy et al.* [2005] found that higher values of VISvs2.12 ratios (e.g., 0.33 and 0.65 for 0.47vs2.12 and 0.66vs2.12, respectively) improved the continuity of the MODIS over-land and over-ocean aerosol products along the coastline of the DelMarVa Peninsula. The MODIS/AERONET τ regression over near-coastal sites was also improved. However, at locations far from the coastline, the CLAMS VISvs2.12 ratios tended toward overcorrection of the surface reflectance and retrievals of τ less than zero. Thus a single set of VISvs2.12 ratios is not globally applicable.

[27] It is known that Earth's surface is not Lambertian and that some surface types exhibit strong bidirectional reflectance functions (BRDF). *Gatebe et al.* [2001] flew the Cloud Absorption Radiometer at low altitudes over different vegetated surfaces and found not only did VISvs2.12 vary by surface type but also as a function of angle. In fact VISvs2.12 ratios often greatly differed from the one-quarter and one-half values assumed for the C004 algorithm. Also, *Remer et al.* [2001] noted that VISvs2.12 varied as a function of scattering geometry. An improved global aerosol retrieval algorithm requires estimates of surface reflectance that include surface type and angular variability.

[28] We explored surface type models and global maps of measured spectral albedo (like those described by *Moody et al.* [2005]) but found that they were not necessarily representative of the directional surface reflectance. Yet we possessed 4 years of colocated MODIS and AERONET data that could be used for developing empirical surface reflectance relationships. Before Terra launch such data were unavailable.

4.1. Atmospheric Correction of MODIS/AERONET Colocated Products

[29] Atmospheric correction [*Kaufman and Sendra*, 1988] attempts to calculate the optical properties of the surface, by theoretically subtracting the effects of the atmosphere from the satellite-observed radiation field. One needs to assume the optical properties of the intervening atmosphere, including all aerosol and nonaerosol components. In addition to knowing or assuming all atmospheric components, accurate radiative transfer (RT) is also required. The atmospherically corrected surface reflectance $\rho^s{}_\lambda$ is calculated by rearranging equation (1).

[30] In order to minimize errors arising from multiple scattering by the aerosol, we should limit our atmospheric corrections to conditions of low τ. Out of the original 15,000 colocated MODIS/AERONET points (described in section 2), there were over 10,000 collocations with low τ ($\tau_{0.55} < 0.2$). The archive included the "gas absorption corrected" MODIS-Level 2 observed reflectance, as well as AERONET-observed (L2A) spectral τ_λ and column water vapor depth. For atmospheric correction, we used the spectral reflectance from the single MODIS 10 km box that contains the AERONET instrument. Aerosol and water vapor characteristics are provided by the closest (in time) AERONET observation to MODIS overpass. The molecular properties of the atmosphere were assumed those of the *U.S. Government Printing Office* [1976], with the Rayleigh optical depth (ROD) values scaled from sea level values, according to the elevation/air pressure of the Sun photometer (details are in the ATBD-2006).

[31] The relation between the satellite-measured reflectance and the surface reflectance is a complicated function of the atmospheric effects of scattering and absorption by the aerosol. Previous atmospheric correction exercises often assumed some form of the Continental aerosol model [e.g., *Vermote et al.*, 1997], to describe both the scattering and absorption properties. While this model may provide reasonable simulations in channels near to 0.55 μm (such as 0.47 and 0.66 μm), it cannot be expected to provide accurate simulations at 2.12 μm, even for low τ. For example, for $\tau_{0.55} = 0.2$, $\tau_{2.12}$ ranges from 0.03 to 0.16, depending on whether fine or coarse dominated aerosol is assumed. Thus assuming the wrong aerosol size in the correction procedure will lead to errors in estimating 2.12 μm surface reflectance.

[32] Therefore we used the AERONET-derived Ångstrom exponent (α) to decide which aerosol type to assume. In the 4200 cases where $\alpha > 1.6$, the atmospheric correction assumed a fine-dominated model, specifically the "moderately absorbing" model ($\omega_0 \sim 0.9$). When $\alpha < 0.6$ (400 cases), the correction procedure assumed the coarse-dominated model. Colocations where $0.6 < \alpha < 1.6$ (about 6000 cases) were not used due to uncertainties of aerosol mixing.

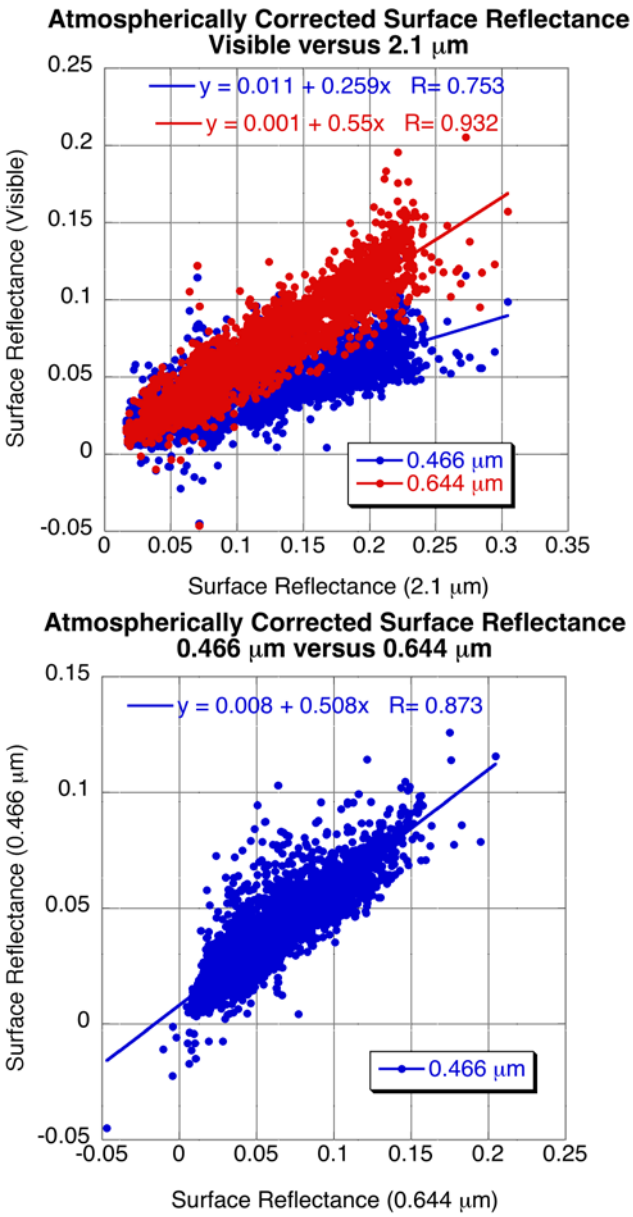

Figure 1. Atmospherically corrected surface reflectance in (a) the visible (0.47 and 0.66 μm channels) compared with that in the 2.12 μm SWIR channel and (b) the 0.47 μm compared with that in the 0.66 μm channel.

[33] The atmospheric correction resulted in two datasets: surface reflectance at three wavelengths (0.47, 0.66, 2.12 μm) for each of the two regimes (fine and coarse-dominated). Separate comparison of 0.66 μm versus 2.12 μm and 0.47 μm versus 2.12 μm, for each regime indicated that their regressions differed by less than 10% (both slope and y-offset values), suggesting to combine the two surface reflectance datasets into one.

4.2. Mean Values of VISvs2.12 Surface Reflectance Relationships

[34] Atmospheric correction was performed on the 4600 MODIS/AERONET co-locations having AERONET-observed $\tau_{0.55} < 0.2$ and either $\alpha < 0.6$ or $\alpha > 1.6$. Figure 1a plots the regressions of corrected 0.47 μm and 0.66 μm surface reflectance, each versus the corrected 2.12 μm surface reflectance. Note both slope and y-offset. The presence of the y-offset is important, because even in the darkest, most water-laden vegetation, zero reflectance at 2.12 μm does not imply zero surface reflectance in the visible channels [e.g., *Kaufman et al.*, 2002].

[35] Correlation (R) values are 0.93 for the 0.66vs2.12 μm channel regression, but only about 0.75 for 0.47vs2.12. For 0.47vs2.12, including the offset (about +0.011) yields a slope close to one-quarter (0.258). For 0.66vs2.12, the offset is near zero, but the slope is greater than one-half (0.55). Thus in a mean sense, atmospheric correction of MODIS data yields VISvs2.12 surface reflectance relationships that differ from the assumed C004 VISvs2.12 ratios.

[36] The relationship of 0.47 to 0.66 μm ("0.47vs0.66") may be stronger than 0.47vs2.12 because it has higher correlation (R = 0.87) and less scatter (Figure 1b). This suggests that we should estimate 0.47 μm surface reflectance indirectly from 0.66 μm, rather than directly from 2.12 μm. In other words, the algorithm should first estimate 0.66 μm from 2.12 μm, then estimate 0.47 μm from 0.66 μm, i.e.,

$$\begin{aligned} \rho^s_{0.66} &= f\left(\rho^s_{2.12}\right) \\ \rho^s_{0.47} &= g\left(\rho^s_{0.66}\right) \end{aligned}, \tag{5}$$

where f() and g() are different relationships. To test whether the relationships shown in Figure 1 are dependent on the formulation data set, we performed similar regressions on a subset of the data where AERONET-measured $\tau < 0.1$ (2508 cases). The results show differences in both slope and y-offset of less than 1%, suggesting that the average VISvs2.12 relationship of equation (5) is robust.

4.3. Variability of VISvs2.12 Surface Reflectance Relationships: Angle

[37] As shown by Figure 1, the VISvs2.12 surface reflectance relationship displays large scatter. For example, if surface reflectance is 0.15 at 2.12 μm, applying the regressed relationships of 0.66vs2.12 and 0.47vs0.66 results in estimates of surface reflectance of 0.083 ± 0.03 at 0.66 μm and 0.050 ± 0.03 at 0.47 μm. Obviously, this could result in very large errors in retrieved τ, on the order of 0.3 or more. Therefore to reduce the scatter we look for dependencies on other parameters to refine the relationships.

[38] A number of papers suggest that the VISvs2.12 surface reflectance relationships are angle dependent [e.g., *Remer et al.*, 2001; *Gatebe et al.*, 2001; *Lyapustin*, 2001]. Out of different possible angle parameters (solar zenith angle, sensor zenith angle, glint angle or scattering angle) we found that the scattering angle had the largest influence on the VISvs2.12 relationship. The scattering angle, Θ, is defined as

$$\Theta = \cos^{-1}\left(-\cos\theta_0\cos\theta + \sin\theta_0\sin\theta\cos\phi\right) \tag{6}$$

where θ_0, θ, and φ are the solar zenith, sensor view zenith, and relative azimuth angles, respectively.

[39] The data from Figure 1 were sorted according to scattering angle and put into 20 groups of equal size (about 230 points for each scattering angle bin). Figure 2a displays

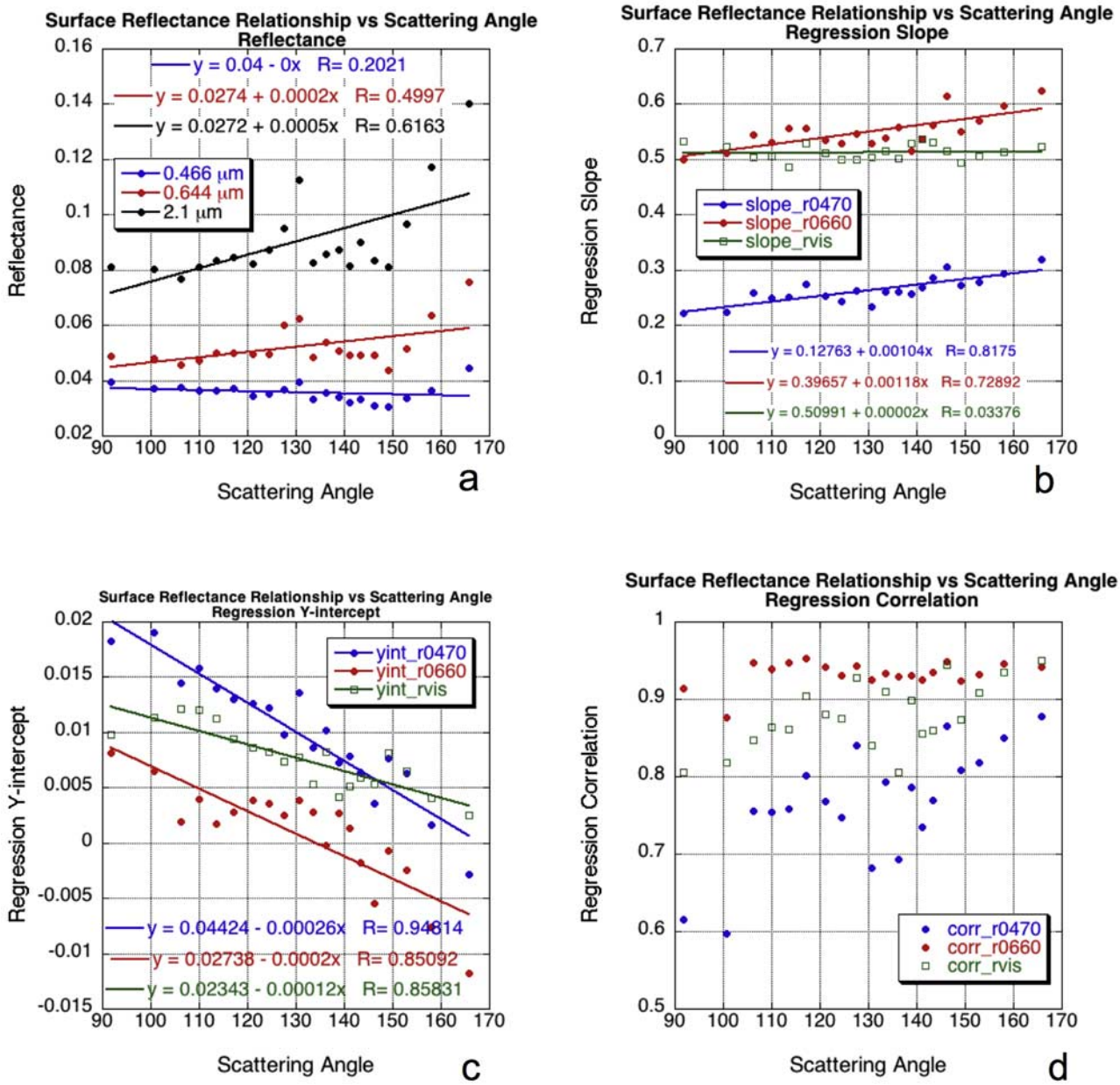

Figure 2. VISvs2.12 surface reflectance relationships as a function of scattering angle. The data were sorted according to scattering angle and put into 20 groups of equal size (about 230 points for each scattering angle bin). On all subplots, each point is plotted for the median value of scattering angle in the bin. Shown are (a) median values of reflectance at each channel as a function of the scattering angle. Linear regression was calculated for the 230 points in each group. Also shown are (b) the slope of the regression (for each angle bin), (c) the y-intercept, and (d) the regression correlation. Note for Figures 2b, 2c, and 2d that 0.47 μm versus 2.12 μm (r0470) is plotted in blue, 0.66 μm versus 2.12 μm (r0660) is plotted in red, and 0.47 versus 0.66 μm (rvis) is plotted in green.

the median values of surface reflectance in each bin as a function of scattering angle and shows a definite relationship at 2.12 μm, less at 0.66 μm, and nearly none at 0.47 μm. Since Figure 1 shows a slope and y-offset for both VISvs2.12 relationships, we look for scattering angle dependence on each slope and y-offset. Figures 2b–2d plots the slope, y-offset, and correlation of the surface reflectance relationships calculated in each scattering angle bin and plotted as a function of scattering angle. The 0.66vs2.12 regression slope (r0660 in the figure) shows dependence on scattering angle, whereas the 0.47vs0.66 regression slope (rVIS in the figure) shows nearly none. Both y-intercepts show strong dependence on scattering angle.

4.4. Variability of VISvs2.12 Surface Reflectance Relationships: Surface Type and $NDVI_{SWIR}$

[40] Because AERONET sites are located in different surface type regimes, it could be expected that the

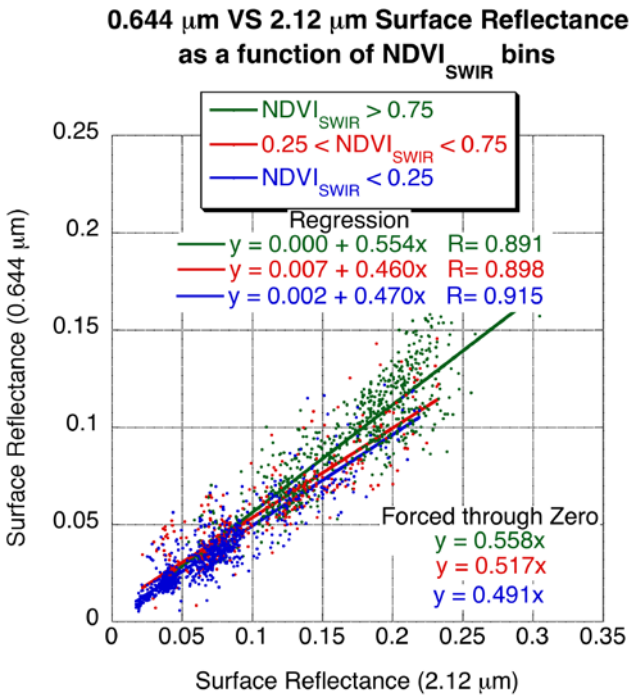

Figure 3. The 0.66 μm versus 2.12 μm surface reflectance as a function of bins of $NDVI_{SWIR}$ values. The standard regression is plotted, with regression equations given in the lower right-hand corner. The ratios (if forced through zero) are given beneath the legend. Blue refers to low $NDVI_{SWIR}$, red to medium and green to high values.

VISvs2.12 surface relationships will vary based on surface type and/or season. Using the International Geosphere/Biosphere Programme's (IGBP) scene map of USGS surface types and formatted for MODIS validation (http://edcdaac.usgs.gov/modis/mod12c1v4.asp), we determined the scene type of the MODIS/AERONET validation box. We then separated urban from nonurban surfaces, and grouped into season (winter or summer) and general location (midlatitude or tropical). We found that different surface types display different VISvs2.12 ratios (also noting the complete regression including slope and y-intercept). Generally, more vegetated surfaces (midlatitude summer sites both urban and nonurban) have higher 0.66vs2.12 surface reflectance ratios (ratio > 0.55) than winter sites or tropical savannas and grasslands (ratio < 0.55). Except for the urban sites during summer (ratio $\sim$ 0.766), the 0.47vs0.66 surface reflectance ratio is relatively consistent (ratio $\sim$ 0.52). The relationship of the surface reflectance ratios to known surface condition suggests a relationship to its vegetation amount/condition or "greenness."

[41] Except for urban areas, most surfaces seem to have VISvs2.12 surface reflectance relationships that may be related to a vegetation index (VI). The well-known Normalized Difference Vegetation Index (NDVI), defined as a function of the red (0.66 μm – channel 1) and near-IR (0.86 μm – channel 2), are influenced by aerosol, negating its usefulness for determining surface type. We attempted to work with other Vis (such as described by *Karnieli et al.* [2001]) that have different sensitivity to atmospheric (aerosol) conditions, and found the most promising to be the $NDVI_{SWIR}$, defined as

$$NDVI_{SWIR} = \left(\rho^m_{1.24} - \rho^m_{2.12}\right)/\left(\rho^m_{1.24} + \rho^m_{2.12}\right) \tag{7}$$

where $\rho_{1.24}$ and $\rho_{2.12}$ are the MODIS-measured reflectances of the 1.24 μm channel (MODIS channel 5) and the 2.12 μm channel (channel 7). These longer wavelengths are much less influenced by aerosol (except for heavy aerosol or dusts) and thus are potentially most useful for estimating surface condition. This VI is also known as $NDVI_{MIR}$ (midinfrared) [e.g., *Karnieli et al.*, 2001]. In aerosol free conditions $NDVI_{SWIR}$ is highly correlated with regular $NDVI$. A value of $NDVI_{SWIR} > 0.6$ is relative to more active vegetation, whereas $NDVI_{SWIR} < 0.2$ is representative of dormant or sparse vegetation. Figure 3 plots the relationship of the 0.66 μm channel and 2.12 μm channel (atmospherically corrected) surface reflectance relationship, for nonurban sites, as a function of low, medium, and high values of $NDVI_{SWIR}$. As the $NDVI_{SWIR}$ increases, the ratio between 0.66 μm and 2.12 μm surface reflectance increases, and we will use this relationship in the final VISvs2.12 surface reflectance parameterization.

4.5. Final Parameterization of VISvs2.12 Surface Reflectance Relationships

[42] Results of the global atmospheric correction exercise imply that not only do the VISvs2.12 surface relationships differ from the ratios assumed by the C004 algorithm, they also have a strong dependence on both geometry and surface type. The VISvs2.12 surface reflectance relationship is parameterized as a function of both $NDVI_{SWIR}$ and scattering angle Θ, such that equation (5) can be expanded:

$$\begin{aligned} \rho^s_{0.66} &= f\left(\rho^s_{2.12}\right) = \rho^s_{2.12} * slope_{0.66/2.12} + yint_{0.66/2.12} \\ &\text{and} \\ \rho^s_{0.47} &= g\left(\rho^s_{0.66}\right) = \rho^s_{0.66} * slope_{0.47/0.66} + yint_{0.47/0.66} \end{aligned} \tag{8}$$

where

$$\begin{aligned} slope_{0.66/2.12} &= slope^{NDVI_{SWIR}}_{0.66/2.12} + 0.002\Theta - 0.27, \\ yint_{0.66/2.12} &= -0.00025\Theta + 0.033, \\ slope_{0.47/0.66} &= 0.49, \text{ and} \\ yint_{0.47/0.66} &= 0.005 \end{aligned} \tag{9}$$

where in turn

$$\begin{aligned} slope^{NDVI_{SWIR}}_{0.66/2.12} &= 0.48; NDVI_{SWIR} < 0.25, \\ slope^{NDVI_{SWIR}}_{0.66/2.12} &= 0.58; NDVI_{SWIR} > 0.75 \\ slope^{NDVI_{SWIR}}_{0.66/2.12} &= 0.48 + 0.2(NDVI_{SWIR} - 0.25); \\ 0.25 &\le NDVI_{SWIR} \le 0.75 \end{aligned} \tag{10}$$

We can consider the relationships described by Figure 1 as global average relationships and the above parameterization for describing perturbations for angle and land type. Note that while the above parameterization in equations (8)–(10) was based on the results of Figures 1–3, the coefficients are not identical to those shown in the figures. The atmospheric corrected data set is the broadest and most comprehensive representation of global surface reflectance relationships,

still it is limited to AERONET site locations, which in turn are mostly concentrated in certain geographical regions (http://aeronet.gsfc.nasa.gov). Trial and error was used to modify the basic results from the AERONET-based atmospheric correction, to give more realistic MODIS retrievals globally (especially in places were few or no AERONET sites are located). We expect the parameterization to derive more accurate estimates of surface reflectance on average than those estimated using fixed ratios.

4.6. Notes on VISvs2.12 Surface Reflectance Relationship Errors

[43] We note that even with the surface reflectance parameterization, there still will be errors in estimating surface reflectance. According to the MODIS Land Surface Reflectance Homepage (http://modis-sr.ltdri.org/html/prodacc.htm), improper aerosol model assumptions can lead to errors in atmospherically corrected reflectance on the order of 0.002 in the 0.47 and 0.66 μm channels and 0.006 at 2.12 μm. The errors are especially large at 2.12 μm due to potentially choosing a fine-dominated model instead of a coarse-dominated model (or vice versa). However, since our study predetermined the choice of fine or coarse-dominated aerosol models via the AERONET-observed Ångstrom exponent, errors at 2.12 μm should be much less, dependent on the choice of fine-dominated aerosol model. For $\tau_{0.55} = 0.5$, the difference in spectral optical thickness between the moderately absorbing model ($\omega_0 \sim 0.90$) and absorbing model ($\omega_0 \sim 0.85$) is about 0.02, 0.02, and 0.002, respectively, in the 0.47, 0.66, and 2.12 μm channels (see ATBD-2006). On average, this would be equivalent to errors of about 0.002, 0.002, and 0.0002, respectively, in surface reflectance but would vary according to the differences in phase function. Regardless, the error at 2.12 μm is small enough so that the derived surface reflectance relationship should be reasonably robust, even when a model with wrong ω_0 was assumed.

[44] Of course, other errors may creep into the surface reflectance parameterization. These include but are not limited to additional surface BRDF effects lost during averaging over scattering angle and errors due to MODIS instrument calibration. The MODIS Land Surface Reflectance Homepage suggests that these errors can cause reflectance errors that are similar in magnitude to those caused by improper aerosol model assumptions.

5. Inversion of Spectral Reflectance, Including 2.12 μm

[45] A major limitation of the C004 algorithms was that aerosol is assumed transparent in the 2.12 μm channel. Under a dust aerosol regime, aerosol transparency is an extremely poor assumption. Even in a fine aerosol dominated regime, τ is not zero. For the moderately absorbing aerosol model ($\omega_0 \sim 0.90$), $\tau_{0.55} = 0.5$ corresponds to $\tau_{2.12} \sim 0.05$, corresponding to an error in 2.12 μm path reflectance of about 0.005. Via the VISvs2.12 reflectance relationship, the path reflectance error at 0.66 μm is on the order of 0.003, leading to $\sim$0.03 error in retrieved τ. As a percentage of the actual τ, the error is not very large. However, combined with errors at 0.47 μm, the resulting error in spectral dependence leads to error in estimating η.

[46] In the spirit of the MODIS aerosol over ocean algorithm [*Tanré et al.*, 1997], we developed a multichannel reflectance inversion for retrieving aerosol properties over land. Analogous to the ocean algorithm's combination of fine and coarse aerosol modes, our new land algorithm attempts to combine fine-dominated and coarse-dominated aerosol models (each bimodal) to match with the observed spectral reflectance. The 2.12 μm channel is assumed to contain both surface and aerosol information, and the visible surface reflectance is a function of the VISvs2.12 surface reflectance relationships we derived in section 4. Simultaneously inverting the aerosol and surface information in the three channels (0.47 μm, 0.66 μm, and 2.12 μm) yields something greater than two pieces of information. With some assumptions, we can derive three parameters: $\tau_{0.55}$, $\eta_{0.55}$, and the surface reflectance ($\rho^s_{2.12}$).

[47] We rewrite equation (1) but note that the calculated spectral total reflectance ρ^*_λ at the top of the atmosphere is the weighted sum of the spectral reflectance from a combination of fine and coarse-dominated aerosol models, i.e.,

$$\rho^*_\lambda = \eta\rho^{*f}_\lambda + (1-\eta)\rho^{*c}_\lambda \tag{11}$$

where ρ^{*f}_λ and ρ^{*c}_λ are each composites of surface reflectance ρ^s_λ and atmospheric path reflectance of the separate aerosol models. That is:

$$\rho^{*f}_\lambda = \rho^{af}_\lambda + F^f_{d\lambda}T^f_\lambda\rho^s_\lambda / \left(1 - s^f_\lambda\rho^s_\lambda\right)$$
$$\text{and} \tag{12}$$
$$\rho^{*c}_\lambda = \rho^{ac}_\lambda + F^c_{d\lambda}T^c_\lambda\rho^s_\lambda / \left(1 - s^c_\lambda\rho^s_\lambda\right)$$

where ρ^{af}_λ and ρ^{ac}_λ are the fine and coarse model atmospheric path reflectance, $F^f_{d\lambda}$ and $F^c_{d\lambda}$ are normalized downward fluxes for zero surface reflectance, T^f_λ and T^c_λ represent upward total transmission into the satellite field of view, and s^f_λ and s^c_λ are atmospheric backscattering ratios. The weighting parameter, η (in equation (11)) is defined for $\lambda = 0.55$ μm. The appendix of *Remer et al.* [2005] describes how this parameter also represents the fraction of the total optical thickness at 0.55 μm contributed by fine (nondust) aerosol. Note the angular and τ dependence of some of the terms $\rho^a = \rho^a(\tau, \theta_0, \theta, \varphi)$, $F = F(\tau, \theta_0)$, $T = T(\tau\tau, \theta)$, $s = s(\tau)$, and $\rho^s = \rho^s(\theta_0, \theta, \varphi)$, whereas the other terms are a function of the aerosol properties (not aerosol amount or geometry) and are contained within the LUT. The surface reflectance is independent of the aerosol but dependent on the geometry. In practical terms, we parameterize the surface reflectance using the VISvs2.12 surface reflectance relationships, which assumes it is a function of scattering angle and vegetation index.

[48] Owing to the limited set of aerosol optical properties in the lookup table, the equations may not have exact solutions and solutions may not be unique. Therefore we find the aerosol solution most closely resembling the set of MODIS measured reflectance. In order to reduce the possibility of nonunique retrievals, we only allow discrete values of η. Upon completion, the retrieval is assigned a Quality Assurance "confidence" (QAC) value that ranges from 0 (bad quality) to 3 (good quality). This QAC flag is used for creation of Level 3 (gridded) products and for combining land retrievals with concurrent over-ocean aerosol retrievals into "joint products" (see ATBD-2006 for more details).

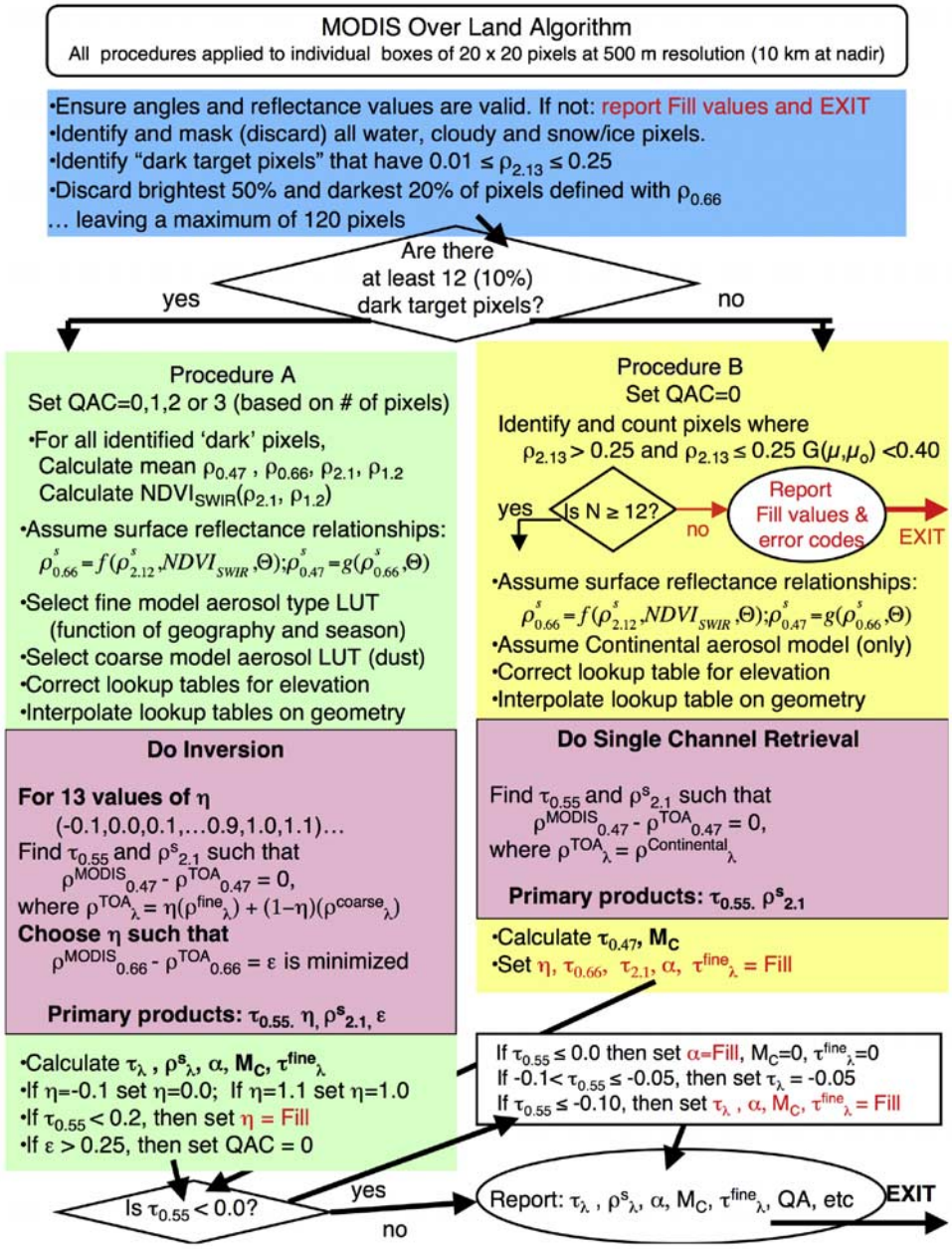

Figure 4. Flowchart illustrating the derivation of aerosol over land for C005.

5.1. Selection of "Dark Pixels"

[49] Figure 4 illustrates the main steps of our new land algorithm. Each individual MODIS scene, called a granule, consists of a 5-min swath of data, measuring approximately 1340 km by 2030 km. The relevant Level 1 B (L1B) data include calibrated spectral reflectance in eight wavelength bands at a variety of spatial resolutions, as well as the associated geolocation information. The spectral data include the 0.66 and 0.86 μm channels (MODIS channels 1 and 2 at 250 m resolution), the 0.47, 0.55, 1.24, 1.64, and 2.12 μm channels (channels 3, 4, 5, 6, and 7 at 500 m), and the 1.38 μm channel (channel 26 at 1 km). The geolocation data are at 1 km and include angles (θ_0, θ, φ, and Θ), latitude, longitude, elevation, and date. L1B reflectance values are corrected for water vapor, ozone, and carbon dioxide (described in ATBD-2006) before proceeding.

[50] The first step is to organize the measured reflectance into nominal 10 km by 10 km boxes (corresponding to 20 by 20, or 40 by 40 pixels, depending on the channel). The 400 pixels in the box are evaluated pixel by pixel to identify whether the pixel is suitable for aerosol retrieval. Clouds [*Martins et al.*, 2002], snow/ice [*Li et al.*, 2005], and inland water bodies (via NDVI tests) are considered not suitable and are discarded. Details of this masking are also described in ATBD-2006.

[51] The nonmasked pixels are checked for their brightness. Pixels having measured 2.12 μm reflectance between 0.01 and 0.25 are grouped and sorted by their 0.66 μm reflectance. The brightest (at 0.66 μm) 50% and darkest 20% are discarded, in order to reduce cloud and surface contamination and scale toward darker targets in the visible wavelengths. If there are at least 12 pixels remaining (10%

of 30% of the original 400), then the reflectance in each channel is averaged, yielding the "MODIS-measured" spectral reflectance $\rho^m_{0.47}$, $\rho^m_{0.66}$, $\rho^m_{2.12}$, and $\rho^m_{1.24}$. These reflectance values are used for Procedure A. If less then 12 pixels remain, then Procedure B (described later) is followed.

5.2. Correcting the LUT for Elevation

[52] A major change from the C004 algorithm concerns how to correct for elevated surface targets. The sea-level Rayleigh optical depth (*ROD*, $\tau_{R,\lambda}$) at a wavelength λ (in μm) can be approximated over the visible range [e.g., *Dutton et al.*, 1994; *Bodhaine et al.*, 1999] by

$$\tau_{R,\lambda} = -0.00877\lambda^{-4.05} \tag{13}$$

When not at sea level (pressure = 1013 mb), the ROD is a function of pressure (or height, z) so that it can be approximated by:

$$\tau_{R,\lambda}(z = Z) = \tau_{R,\lambda}(z = 0)\exp\left(\frac{-Z}{8.5}\right) \tag{14}$$

where Z is the height (in kilometers) of the surface target and 8.5 km is the exponential scale height of the atmosphere. The difference between ROD at z = 0 and z = Z is $\Delta\tau_{R,\lambda}$.

[53] In C004, the algorithm (too) simply corrected the retrieved τ product by adding the optical depth that was neglected by assuming sea level for the retrieval, (i.e. $\tau_\lambda(z = Z) = \tau_\lambda(z = 0) + \Delta\tau_{R,\lambda}$). However, this correction can give poor results because of the large differences between molecular and aerosol phase functions. Instead, we use the procedure described by *Fraser et al.* [1989], adjusting the lookup table to simulate different ROD by adjusting the wavelength. Substitution of equation (13) into equation (14) yields

$$\lambda(z = Z) = \lambda(z = 0)\exp\left(\frac{Z}{34}\right). \tag{15}$$

[54] For example, at Z = 0.4 km, λ increases by about 1.2%. For the blue 0.47 μm channel (centered at 0.466 μm) this means that $\tau_{R,\lambda}(z = 0) = 0.194$, $\tau_{R,\lambda}(z = 0.4) = 0.185$ and $\lambda(z = 0.4) = 0.471$ μm. In other words, the algorithm simulates an 0.4 km elevated surface by adjusting the blue channel's wavelength to 0.471 μm. Assuming that gases and aerosols are optically well mixed in altitude, the parameter values of a 0.471 μm LUT can be acquired by interpolating (linearly as functions of log wavelength and log parameter) between the 0.47 μm (0.466 μm) and the 0.55 μm (0.553 μm) entries. Similar interpolations are performed for the other channels (for example, 0.55 μm would be adjusted to 0.559 μm). For the 0.4 km case, this means that lower values of TOA atmospheric path reflectance and higher values of transmission are chosen to represent a given aerosol model's optical contribution. However, also note that since the 0.55 μm channel has also been adjusted, the associated values of the τ indices have been adjusted accordingly. In other words, the algorithm retrieves aerosol optical depth at the adjusted wavelength, which is equivalent to retrieving τ down to the surface elevation height. For highly elevated terrain (e.g., Z = 4 km), ROD decreases by 40%, resulting in a channel equivalent wavelength increase of 10%.

[55] Whereas most global land surfaces are at sea level or above, a few locations are below sea level (Z < 0). In these cases, the algorithm is allowed to extrapolate below 0.466 μm. Since the extrapolation is at most for 100 m or so, this is not expected to introduce large errors, and these cases can still be retrieved. Note also that due to the extremely low ROD in the 2.12 μm channel, little is gained by adjusting this channel.

5.3. Procedure A: Inversion for Dark Surfaces

[56] If following Procedure A (for dark surfaces), the QAC is initially set to a value between 0 (bad quality) and 3 (good quality), depending on the number of dark pixels remaining. In Procedure A the algorithm assigns the fine aerosol model, based on the location and time (*Levy et al.* [2007], ATBD-2006). From the lookup table, ρ^a, F, T, and s (for the fine model and coarse model separately) are interpolated for angles (θ_0, θ, and φ), resulting in six values for each parameter, each one corresponding to a different aerosol loading (indexed by τ at 0.55 μm).

[57] The 2.12 μm path reflectance is a nonnegligible function of τ (for example, for the nonabsorbing aerosol model, $\tau_{0.55}$ = 0.5 corresponds to $\tau_{2.12}$ = 0.05), so the surface reflectance is therefore also a function of τ. For discrete values of η between −0.1 and 1.1 (intervals of 0.1), the algorithm attempts to find the τ at 0.55 μm and the surface reflectance at 2.12 μm that exactly matches the MODIS measured reflectance at 0.47 μm. There will be some error, ε, at 0.66 μm. The solution is the one where the fitting error at 0.66 μm is minimized. In other words,

$$ABS\left(\rho^*_{0.47} - \rho^m_{0.47}\right)/\rho^m_{0.47} = 0 \tag{16a}$$

$$ABS\left(\rho^*_{0.66} - \rho^m_{0.66}\right)/\rho^m_{0.66} = \varepsilon \tag{16b}$$

$$ABS\left(\rho^*_{2.12} - \rho^m_{2.12}\right)/\rho^m_{2.12} = 0 \tag{16c}$$

where

$$\begin{aligned}\rho^*_{2.12} = {} & \eta\left(\rho^{fa}_{2.12} + F^f_{d,2.12}T^f_{2.12}\rho^f_{2.12}/\left(1 - s^f_{2.12}\rho^s_{2.12}\right)\right) \\ & +(1-\eta)\left(\rho^{ca}_{2.12} + F^c_{d,2.12}T^c_{2.12}\rho^s_{2.12}/\left(1 - s^c_{2.12}\rho^s_{2.12}\right)\right)\end{aligned} \tag{17a}$$

$$\begin{aligned}\rho^*_{0.66} = {} & \eta\left(\rho^{fa}_{0.66} + F^f_{d,0.66}T^f_{0.66}f\left(\rho^s_{2.12}\right)/\left(1 - s^f_{0.66}f\left(\rho^s_{2.12}\right)\right)\right) \\ & +(1-\eta)\left(\rho^{ca}_{0.66} + F^c_{d,0.66}T^c_{0.66}f\left(\rho^s_{2.12}\right)/\left(1 - s^c_{0.66}f\left(\rho^s_{2.12}\right)\right)\right)\end{aligned}$$

and (17b)

$$\begin{aligned}\rho^*_{0.47} = {} & \eta\left(\rho^{fa}_{0.47} + F^f_{d,0.47}T^f_{0.47}g\left(\rho^s_{0.66}\right)/\left(1 - s^f_{0.47}g\left(\rho^s_{0.66}\right)\right)\right) \\ & +(1-\eta)\left(\rho^{ca}_{0.47} + F^c_{d,0.47}T^c_{0.47}g\left(\rho^s_{0.66}\right)/\left(1 - s^c_{0.47}g\left(\rho^s_{0.66}\right)\right)\right),\end{aligned} \tag{17c}$$

where, in turn, $\rho^a = \rho^a(\tau)$, $F = F(\tau)$, $T = T(\tau)$, $s = s(\tau)$ are functions of τ indices in the lookup table that is calculated separately for fine and coarse models. $F(\rho^s{}_{2.12})$, $g(\rho^s{}_{0.66})$ are described by equations (8)–(10). Note that nonphysical values of η are tried (−0.1 and 1.1) to allow for the

possibility of inappropriate assumptions in either aerosol models or surface reflectance. Again, the primary products are $\tau_{0.55}$, $\eta_{0.55}$, and the surface reflectance ($\rho^s{}_{2.12}$). The fitting error ε is also noted.

5.4. Procedure B: Alternative Retrieval for Brighter Surfaces

[58] The derivation of aerosol properties is possible when the 2.12 μm reflectance is brighter than 0.25, but is expected to be less accurate [*Remer et al.*, 2005], due to increasing errors in the VISvs2.12 relationship. However, if Procedure A was not possible, but there are at least 12 cloud-screened, nonwater pixels, satisfying

$$0.25 < \rho^m_{2.12} < 0.25G < 0.40 \tag{18}$$

where

$$G = 0.5\left((1/\mu) + \left(1/\sqrt{\mu_0}\right)\right), \tag{19}$$

then Procedure B is attempted. In this relationship μo is cosine of the solar zenith angle, cos(θ_o), and μ is cosine of the satellite view angle, cos(θ). Equation (19) is a representation of the slant path of the radiation. The concept is that at oblique angles, as the photon path increases, more and more signal originates from the atmosphere and less from the land. The contribution from the surface reflectance becomes less important, and the retrieval can tolerate higher surface reflectance [*Remer et al.*, 2005]. In procedure B, the QAC is automatically set to 0 ("bad quality").

[59] Procedure B is analogous to "Path B" described by *Remer et al.* [2005]. Like in C004, the Continental aerosol model is assumed. Unlike C004, the VISvs2.12 surface reflectance assumptions are those described by equations (8)–(10), and the Continental aerosol properties are indexed to 0.55 μm. In other words, it uses equations (11)–(12), except with the first term only (i.e., η = 1.0). The primary products for Procedure B are τ ($\tau_{0.55}$) and the surface reflectance ($\rho^s_{2.12}$). The error ε is also saved.

5.5. Low and Negative Optical Depth Retrievals

[60] A major philosophical change from C004 to C005 is that negative τ retrievals are allowed. Given that there is both positive and negative noise in the MODIS observations, and that surface reflectance and aerosol properties may be underestimated or overestimated depending on the retrieval conditions, it is statistically imperative to allow retrieval of negative τ. In fact it is necessary for creating an unbiased data set from any instrument. Without negative retrievals the τ data set is biased by definition. However, a large negative retrieval indicates a situation outside the algorithm's solution space and should not be reported. The trick is to determine the cutoff between a retrieved τ that is essentially the same as zero, and a retrieved τ that is truly wrong. MODIS should retrieve with the expected error defined by equation (2), then values down to -0.05 are essentially the same as a zero retrieval and are reported as retrieved. Allowing for slightly higher uncertainty, we include τ retrievals down to -0.10 (twice the expected error in pristine aerosol conditions) but report these values as -0.05 and lower the QAC value. Note that all retrievals with $-0.05 < \tau < 0$ are reported with high QAC value = 3, unless identified as poor quality for some other reason. Some of the products that are retrieved or derived (such as η or Ångstrom Exponent) are set to zero or reported as not defined for negative retrievals. In cases of low τ ($\tau < 0.2$), η is too unstable to be retrieved with any accuracy. Therefore η is reported as undefined even though other parameters (such as Ångstrom exponent and Fine τ) may be reported.

5.6. Sensitivity Study

[61] Owing to our collective experience with the C004 family of MODIS aerosol algorithms (both over land and ocean), we found it unnecessary to perform an exhaustive study of the information content (such as done by *Tanré et al.* [1996]). We expect from the use of MODIS channels with wide spectral range, and the assignment of expected aerosol type, that the algorithm (Procedure A) should be able to retrieve τ with robustness, and have some sensitivity to the size parameter η. Following the lead of *Tanré et al.* [1997], we have tested the sensitivity of Procedure A by applying it for the following exercises: (1) simulation of conditions that are included within the LUT, (2) simulations of conditions not included in the LUT, and (3) simulations for conditions that include one or more errors.

5.6.1. Exercise 1

[62] Whereas the study of *Tanré et al.* [1997] tested the algorithm on a single geometrical combination, we simulated the 720 reasonable geometrical combinations in the LUT ($0° \leq \varphi \leq 180°$, $\theta \leq 60°$, $\theta_0 \leq 48°$). We assumed the fine-dominated aerosol model to be the moderately absorbing ($\omega_0 \sim 0.9$) aerosol model and that the coarse-dominated model was our spheroid (dust) model (e.g., *Levy et al.* [2007]; ATBD-2006). For each combination of geometry, and for each MODIS channel, we extracted the fine and coarse mode values of atmospheric path reflectance ρ^a_λ, backscattering ratio s_λ, downward flux F_d and transmission T_λ. We assumed that the 2.12 μm surface reflectance $\rho^s_{2.12}$ = 0.15, and the C004 VISvs2.12 surface reflectance ratios (i.e., $\rho^s_{0.66}$ = 0.5 $\rho^s_{2.12}$ and $\rho^s_{0.47}$ = 0.5$\rho^s_{0.66}$). Using equations (11)–(12), we simulated TOA reflectance ρ^*_λ for five discrete values of η (η = 0.0, 0.25, 0.5, 0.75, and 1.0). Therefore for each value of τ in the LUT, there are 720 × 5 = 3600 attempts to retrieve that τ.

[63] For smaller τ ($\tau \leq 1$), the τ was retrieved within $\Delta\tau < 0.01$ for all 3600 attempts. As τ increases, however, computational instabilities lead to a less exact solution. Still, though, the retrieved τ is certainly within 10% and in most cases to within $\Delta\tau < 0.1$. When we hold τ constant (τ = 0.5) and attempt to retrieve values of η within the LUT (η = 0.0 or 1.0) for the 720 geometrical combinations, we find that η is retrieved exactly (see ATBD-2006 for more details).

[64] Figures 5 and 6 provide another way of assessing the retrieved MODIS products. Figure 5 plots retrieved τ, surface reflectance and fitting error as a function of either air mass (top) or scattering angle (bottom), given that the input conditions are $\tau_{0.55}$ = 0.5, η = 0.5, and $\rho^s{}_{2.12}$ = 0.15. In this case, we plotted all of the 720 geometrical combinations in the LUT. The retrieval never exactly matches the input reflectances, although the errors are very small (less than 0.1%). Note that the retrieval uses an underestimated surface reflectance to balance the overestimated optical

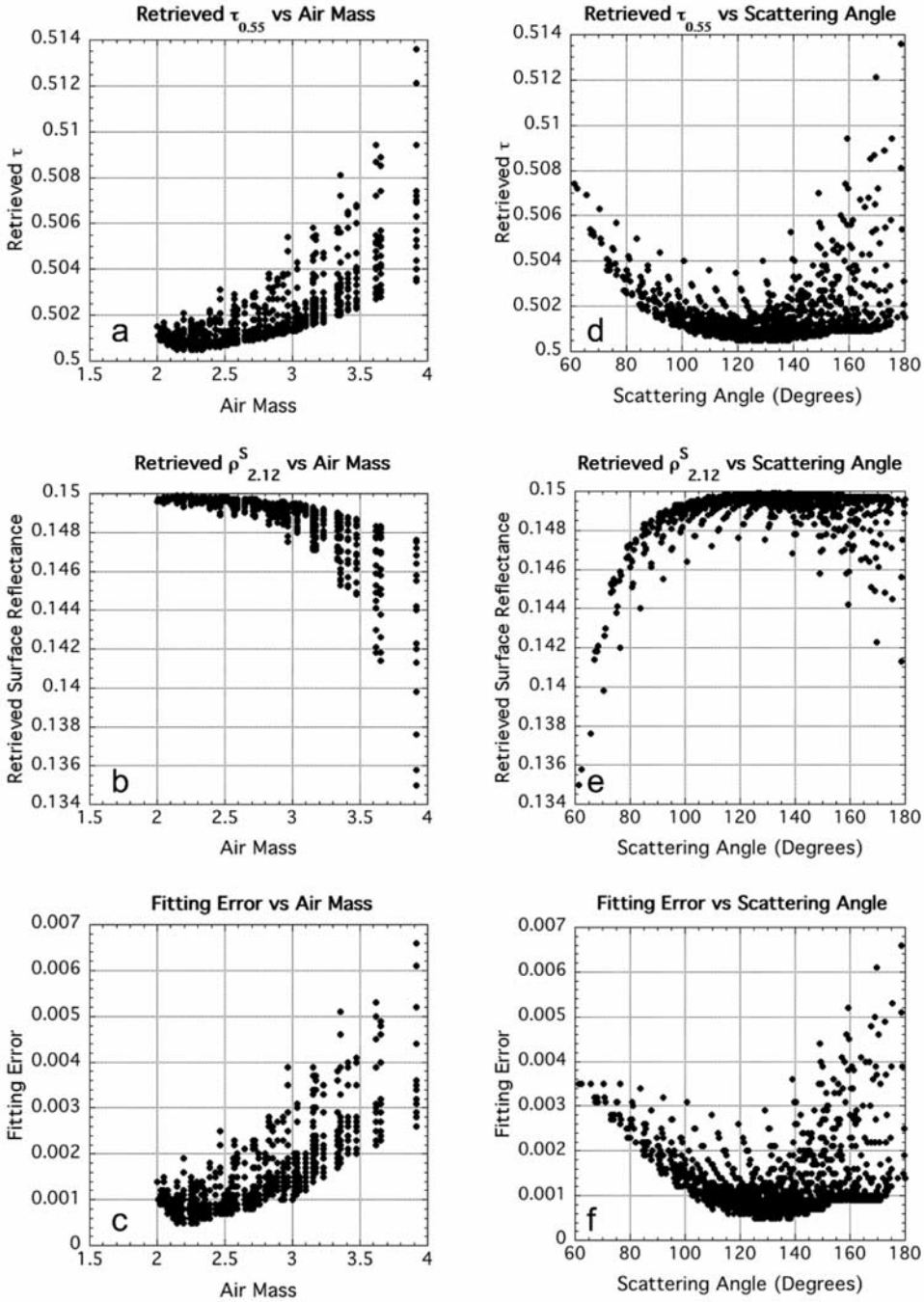

Figure 5. Retrieved Moderate Resolution Imaging Spectroradiometer (MODIS) products as a function of (a–c) air mass and (d–f) scattering angle for inputted atmospheric conditions (τ = 0.5, η = 0.5, and $\rho^{s}_{2.12}$ = 0.15) and 720 LUT geometrical combinations. The retrieved τ is plotted in Figures 5a and 5d, the 2.12 μm surface reflectance is plotted in Figures 5b and 5e, and the fitting error is plotted in Figures 5c and 5f. Note that in all cases, the η value of 0.5 was retrieved exactly.

depth. Fortunately, though, most errors are small and are well within any expected error bars. Figure 6 is similar, but for η = 0.25, and plotted only for the air mass dependence. The errors are much larger (up to 1%), but τ is still well within expected error.

5.6.2. Exercise 2

[65] We used the same combination of radiative transfer codes (MIEV + RT3) used for creating the LUT [*Levy et al.*, 2007] to simulate additional values of aerosol loading ($\tau_{0.55}$ = 0.35, 1.5, and 6.0) to create an "extended" LUT (as compared to the "regular" LUT). As in exercise (1) we simulated the same 720 geometrical combinations with the same five values of η. On average the retrieval is very close to the expected value, however, the standard deviation over all geometry is larger than for τ in the regular LUT. A notable exception is the attempt at retrieving $\tau_{0.55}$ = 6.0, where the algorithm does a poor job of extrapolating. In the operational algorithm, we constrain the maximum possible τ to be 5.0.

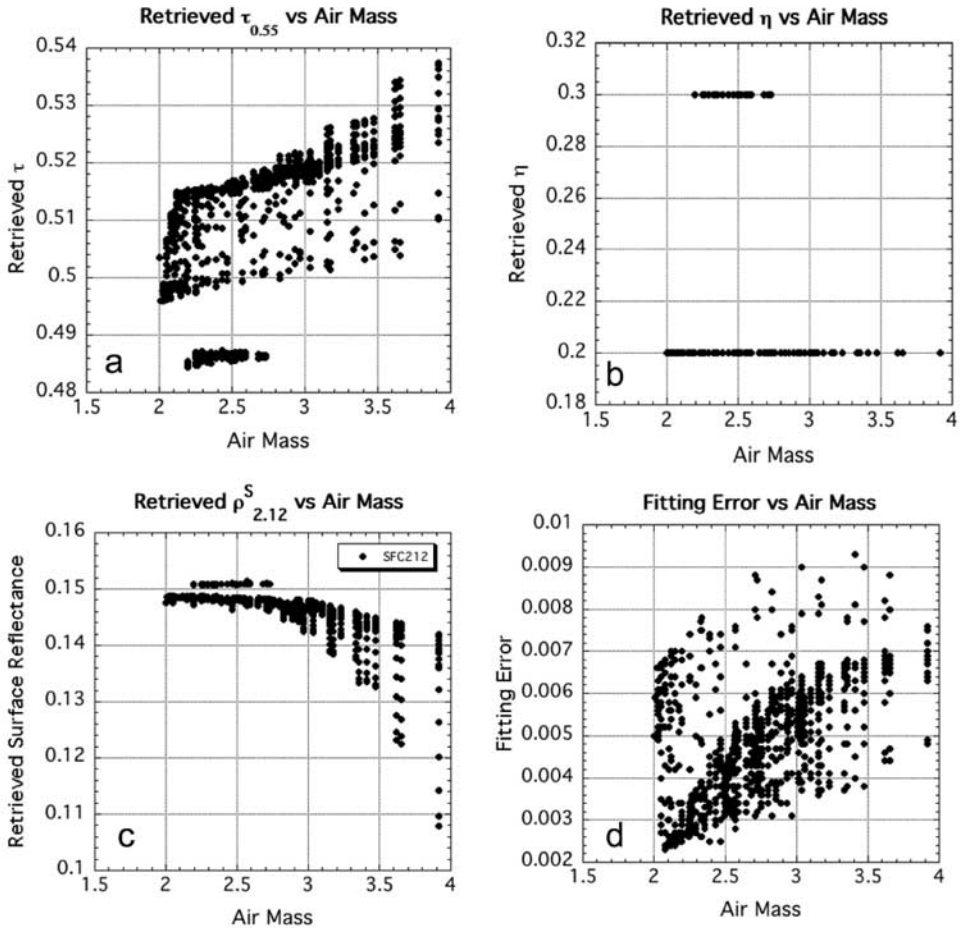

Figure 6. Retrieved MODIS products as a function of air mass for inputted atmospheric conditions (τ = 0.5, η = 0.25, and $\rho^s_{2.12}$ = 0.15) and 720 LUT geometrical combinations. Shown are (a) retrieved τ, (b) retrieved η, (c) the 2.12 μm surface reflectance, and the (d) fitting error is plotted.

As for retrieving values of η not included in the regular LUT, the algorithm is successful. The η = 0.5 retrieval is well behaved. The attempt at resolving either η = 0.25 or η = 0.75 leads to retrieving η = 0.20 and η = 0.70. Although it is impossible for an exact retrieval, due to the algorithm choosing between 0.1 intervals, it is interesting that no retrievals of η = 0.30 or η = 0.80 are produced.

5.6.3. Exercise 3

[66] This exercise studied the impact of different types of errors that could creep into the retrieval process. Potential errors include (but are not limited to) random, systematic, or spectrally dependent errors that arise from issues like sensor calibration, assuming the wrong aerosol model at a given location, coarse input topography mapping, or wrong estimates of the VISvs2.12 surface reflectance relationships. These errors are expressed by adding random or systematic errors in the measurements of one or more spectral channels, geometrical conditions, or other input boundary conditions. Table 2 lists some prescribed errors, and Table 3 lists eight sample geometries used in this exercise. Table 4 shows results when attempting to retrieve conditions of $\tau_{0.55}$ = 0.5, η = 0.5, and $\rho^s_{2.12}$ = 0.15, for the eight sample geometries described in Table 3. Table 4a displays the retrieved values of $\tau_{0.55}$ for each case. Table 4b shows the Mean Squared Error (MSE) for each retrieved product, computed over all eight

Table 2. List of Prescribed Errors for V5.2 Sensitivity Study

Reference	Error Name	Description
1	LUTinput	LUT input: Use the LUT with no prescribed errors
2	ModError	Aerosol model error: We tried to retrieve with the Non-absorbing fine model LUT
3	RndError	Random Error: All channels have random reflectance error of up to ±0.002
4	SfcError	Surface Error: 10% error in assumed 0.66/2.12 surface reflectance relationship
5	CalError	Calibration Error: All channels have random error of up to ±1%
6	ElvError	Elevation Error: Elevation is 1km instead of assumed sea level
7	GeoError	Geometry Error: All angles have random error of up to ±5 degrees
8	AllError	Combination of 2, 3, 4, 5, 6, and 7.

Table 3. Solar/Surface/Satellite Geometry for Eight Examples[a]

Reference	Solar Zenith	View Zenith	Relative Azimuth	Scattering Angle
A	12.00	6.97	60.00	163.40
B	12.00	52.84	60.00	120.53
C	12.00	6.97	120.00	169.59
D	12.00	52.84	120.00	132.35
E	36.00	6.97	60.00	140.12
F	36.00	52.84	60.00	104.74
G	36.00	6.97	120.00	147.00
H	36.00	52.84	120.00	136.29

[a]All units are degrees.

geometries. For any case of prescribed errors/geometry, one or more products may be overestimated or underestimated. If all geometry leads to either one direction or the other, the MSE value is designated by (+) or (−). For example, when retrieving with no additional errors ("LUTinput"), τ is never retrieved exactly but is overestimated by an average MSE of 0.0011 (+). In balance, $\rho^s_{2.12}$ is consistently underestimated (MSE of 0.0004 (−)), with a nonzero fitting error, ε. This is simply a result of computer round off error.

[67] Under most conditions, introducing minor calibration or random errors does not destroy the retrieval of τ. For most individual errors, the retrieved τ is accurate to within 0.02. However, even when we combine errors (model error, random error, surface error, calibration error, and geometrical error), we still retrieve τ = 0.5 with MSE = 0.10, thus retrieving within the expected error of $\Delta\tau = 0.125$. Retrieval of surface reflectance seems to be robust. Retrieval of η is much more unstable. For simple calibration and geometrical errors, the MSE for η is < 0.1. Combinations of errors lead to large MSE (>0.2) for η retrieval, meaning that η is not a stable product. Yet even though the η parameter is sensitive to errors, it can give qualitative indication of particle size.

6. Aerosol Products

[68] Examples of the three primary aerosol products ($\tau_{0.55}$, η, and $\rho^s_{2.12}$) are shown in Figure 7, along with a color composite of the L1B reflectances (0.47, 0.55, and 0.66 μm channels). This image was taken on 4 May 2001 over the U.S. east coast and is the same image used by *King et al.* [2003]. We note the continuity of the τ from land to ocean and that the retrieval of η and surface reflectance seem reasonable. Note that η is not plotted over land when $\tau < 0.2$.

[69] Table 5 lists the aerosol over land products that are contained in each 'M?D04' L2 product file (where the '?' refers to which MODIS sensor is used: 'O' for MOD04/Terra and 'Y' for MYD04/Aqua). For each product, the table lists its name within the file, its dimension, and its type. All products are at least two-dimensional (nominally 135 × 204 at 10 km × 10 km resolution), and many have three dimensions. If there is a third dimension, the channels (usually wavelengths) are listed. A parameter's type may be Retrieved, Derived, Diagnostic, Experimental, or Joint Land and Ocean. A Retrieved parameter is one that results directly from the inversion (Procedure A), whereas those Derived (such as the Ångstrom Exponent), result from those directly retrieved. Products that are Diagnostic include QA parameters and those parameters that were calculated during intermediate steps. These diagnostic parameters can be used to understand how the retrieval worked. Products denoted Experimental are superfluous to the main inversion, may be useful for other applications, but are not discussed here. Finally, Joint Land and Ocean products are those that are composites of over-land and over-ocean aerosol retrievals. These are intended either for quantitative use (Quality Assured where QAC > 0; e.g., Optical_Depth_Land_And_Ocean), or for qualitative imaging (QAC ≥ 0; e.g., Image_Optical_Depth_Land_And_Ocean).

7. Provisional Evaluation of C005

[70] The primary means of MODIS validation is by comparing the products with equivalent measurements from AERONET or other aerosol measurements. In this way, some of the products of C004 (i.e., V4.2 and before) were validated [e.g., *Remer et al.*, 2005], meaning that their uncertainties are quantified. In the case of the land products (through V4.2), this meant that ~60% (slightly less than one standard deviation) of the AERONET-measured τ values were retrieved by MODIS to the expected error described by equation (2). The other land parameters were either not yet validated or are diagnostic parameters that cannot be validated.

[71] Since that paper, the algorithm has gone through some minor updates. The last update to the C004 family was known as Version 5.1 ("V5.1"). V5.1 updated the snow mask [*Li et al.*, 2005] and cleaned up confusing information in the output files. Originally, V5.1 was intended for producing C005; instead it was replaced with the second-generation algorithm (V5.2) described here. Even though V5.1 never became operational, it bridges the C004 and C005 algorithms. In this section, we use both versions (in a nonoperational setting), thereby performing a fair comparison. "V5.1" refers to C004-type products, whereas "V5.2" to C005-type products. In addition to comparison to AERONET retrievals, we make qualitative analyses based on visual inspection and global statistics.

7.1. Direct Comparison of C005 and C004

[72] Figure 8 plots retrieved τ at 0.55 μm from both V5.1 and V5.2, over small areas of a MODIS granule. V5.1 (OLD) is presented in Figure 8a, whereas V5.2 (NEW) is

Table 4a. Results of Sensitivity Study Using Prescribed Errors With Retrieved τ at 0.55 μm (Expected τ = 0.5)

Geometry Error Name	LUTinput	RndError	CalError	GeoError	ModError	ElvError	SfcError	AllError
A	0.501	0.4786	0.5242	0.5143	0.5015	0.6068	0.5402	0.6963
B	0.501	0.4887	0.5242	0.4977	0.4993	0.6035	0.5422	0.6677
C	0.501	0.5227	0.5227	0.4657	0.4835	0.5104	0.4955	0.4809
D	0.5011	0.5104	0.4995	0.4761	0.5014	0.5228	0.498	0.4892
E	0.5008	0.4754	0.502	0.4893	0.4866	0.5211	0.4877	0.5737
F	0.501	0.5135	0.5029	0.4922	0.5035	0.531	0.488	0.5536
G	0.5014	0.4973	0.5199	0.4698	0.4811	0.5097	0.488	0.427
H	0.5016	0.4961	0.5001	0.4744	0.5198	0.5299	0.4939	0.5106

Table 4b. Results of Sensitivity Study Using Prescribed Errors With MSE of Retrieved τ, η, ρ^{σ}, and ε (Expected $\tau = 0.5$, $\eta = 0.5$, $\rho^{\sigma} = 0.15$, and $\varepsilon = 0.0$)[a]

Product Error Name	LUTinput	RndError	CalError	GeoError	ModError	ElvError	SfcError	AllError
τ	0.0011(+)	0.0159	0.0162	0.0215	0.0123	0.0561(+)	0.0221	0.1006
η	0.0000	0.0000	0.0707	0.1000	0.0707	0.4243 (+)	0.1323 (+)	0.4912 (+)
ρ	0.0004 (−)	0.0008	0.0022	0.0025	0.0031 (−)	0.0067	0.0020 (+)	0.0074 (+)
ε	0.0010	0.0021	0.0037	0.0028	0.0020	0.0025	0.0035	0.0052

[a]Entries designated with plus symbol mean that the product was overestimated for all eight geometries, whereas those with a minus symbol means it was underestimated for all geometries.

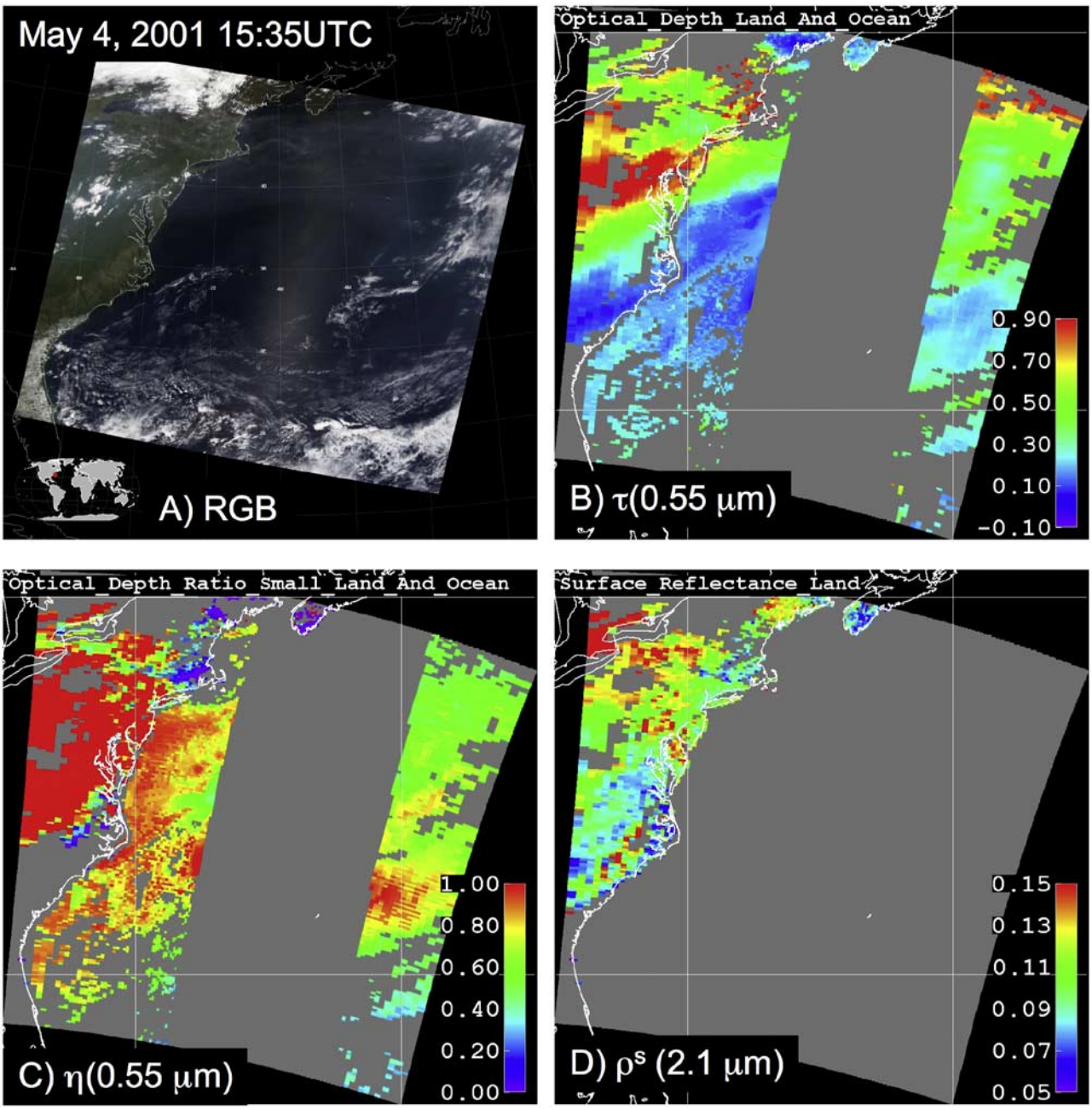

Figure 7. Retrieved aerosol and surface properties over the eastern United States on 4 May 2001. This figure can be compared with that plotted in the work of *King et al.* [2003]. Shown is (a) a "true-color" composite image of three visible channels, showing haze over the mid-Atlantic, and (b–c) retrieved τ and η, showing that the heavy aerosol ($\tau \sim 1.0$) is dominated by fine particles. The transport of the aerosol into the Atlantic is well represented with good agreement between land and ocean. Note that over-land η is not reported when $\tau < 0.2$. Also shown is (d) the retrieved surface reflectance.

Table 5. Contents of MODIS C005 Aerosol Level 2 File (MOD04/MYD04): Land Products[a]

Name of Product (SDS)	Dimesions: Third Dimension	Type of Product
Corrected_Optical_Depth_Land	X,Y,3: 0.47, 0.55, 0.66 μm	Retrieved Primary
Corrected_Optical_Depth_Land_wav2p1	X,Y,1: 2.12 μm	Retrieved Primary
Optical_Depth_Ratio_Small_Land	X,Y: (for 0.55 μm)	Retrieved Primary
Surface_Reflectance_Land	X,Y,3: 0.47, 0.66, 2.12 μm	Retrieved Primary
Fitting_Error_Land	X,Y: (at 0.66 μm)	Retrieved By-Product
Quality_Assurance_Land	X,Y,5: 5 bytes	Diagnostic
Aerosol_Type_Land	X,Y:	Diagnostic
Angstrom_Exponent_Land	X,Y: (for 0.66/0.47 μm)	Derived
Mass_Concentration_Land	X,Y:	Derived
Optical_Depth_Small_Land	X,Y,4: 0.47, 0.55, 0.66, 2.12 μm	Derived
Mean_Reflectance_Land	X,Y,7: 0.47, 0.55, 0.66, 0.86, 1.2, 1.6, 2.12 μm	Diagnostic
STD_Reflectance_Land	X,Y,7: 0.47, 0.55, 0.66, 0.86, 1.2, 1.6, 2.12 μm	Diagnostic
Cloud_Fraction_Land	X,Y:	Diagnostic
Number_Pixels_Used_Land	X,Y:	Diagnostic
Path_Radiance_Land	X,Y,2: 0.47, 0.66 μm	Experimental
Error_Path_Radiance_Land	X,Y,2: 0.47, 0.66 μm	Experimental
Critical_Reflectance_Land	X,Y,2: 0.47, 0.66 μm	Experimental
Error_Crit_Reflectance_land	X,Y,2: 0.47, 0.66 μm	Experimental
Error_Critical_Reflectance_Land	X,Y,2: 0.47, 0.66 μm	Experimental
Quality_Weight_Path_Radiance_Land	X,Y,2: 0.47, 0.66 μm	Experimental
Quality_Weight_Crit_Reflectance_Land	X,Y,2: 0.47, 0.66 μm	Experimental
Optical_Depth_Land_And_Ocean	X,Y: 0.55 μm	Joint Land and Ocean
Image_Optical_Depth_Land_And_Ocean	X,Y: 0.55 μm	Joint Land and Ocean
Optical_Depth_Ratio_Small_Land_And_Ocean	X,Y: 0.55 μm	Joint Land and Ocean

[a]X = 135; Y = 203. If there is a third dimension of the SDS, then the indices of it are given. The "Retrieved" parameters are the solution to the inversion, whereas "Derived" parameters follow from the choice of solution. "Diagnostic" parameters aid in understanding of the directly Retrieved or Derived products. "Experimental" products are unrelated to the inversion but may have future applications. "Joint Land and Ocean" indicate combined land and ocean products.

shown in Figure 8b. Figure 8 shows a region in the western United States from 30 September 2003. The V5.2 aerosol retrieval adds more valid retrievals over very low τ areas (coastal Oregon and northern California). V5.2 reports these areas as having near zero or slightly negative τ, where V5.1 would have reported fill values (no retrieval). In areas farther from the coastline, V5.2 tends to clean up contamination presumably caused by clouds, elevation, and inhomogeneous surface properties and produces a much more reasonable picture of τ.

7.2. Statistics

[73] Of most interest to the climate community will be the changes in the statistics of the aerosol products. These include the global mean values and the distribution (histogram) of the values. For the set of MODIS granules listed in Table 6 (about 6300 granules of both Terra and Aqua), the mean 0.55 μm τ is reduced from 0.28 to 0.21. This is a significant reduction that can be compared with model estimates.

[74] Figure 9 plots the histograms of retrieved τ at 0.55 μm from both V5.1 and V5.2. These histograms include 141 individual Terra and Aqua granules that are known as the MODIS "test_bed" and 12 days of global data, all listed in Table 6. The use of global data is especially important for determining how the retrieval behaves in regions not selected for algorithm development. Of course, the obvious change in the V5.2 product is that small magnitude negative τ retrievals are valid. About 10–11% of the total τ retrievals are now retrieved as below zero, of which only about 3% are below -0.05. This promising result indicates that V5.2 has reasonable ability to detect very clean conditions within the expected error of ± 0.05. Also noted in Figure 9 is that the fraction of retrieved medium to medium high τ ($0.2 < \tau < 0.75$) is reduced, while the fraction of high τ ($\tau > 0.75$) remains about the same.

7.3. Comparison of V5.2 to V5.1 and With AERONET

[75] As of 1 April 2006, the V5.2 algorithm has been run on nearly 6300 granules, including 1 full month (August 2001), 15 entire days (listed in Table 6), and about

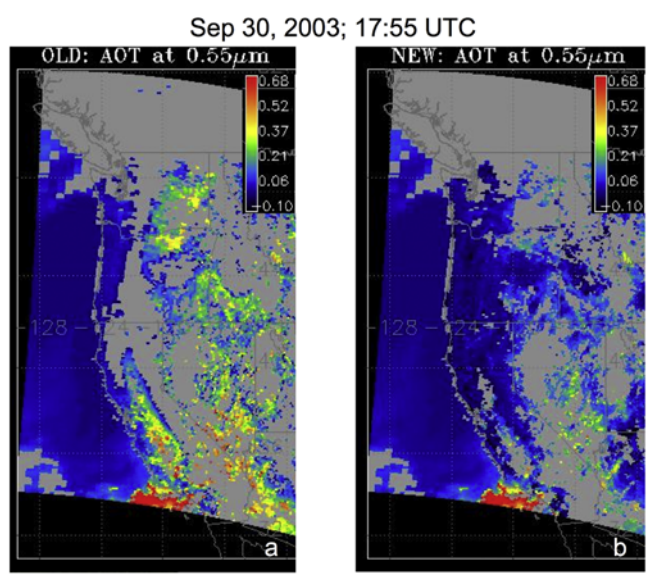

Figure 8. Retrieved τ (AOT) at 0.55 μm for (a) old V5.1 and (b) new V5.2 over California for 30 September 2003. The color scale is the same for both plots. Note the increase in the retrieval spatial coverage and reduction in surface contamination for V5.2.

Table 6. Description of Data Used in C005 Provisional Validation[a]

Date of MODIS Observations	Terra/Aqua	Why Interesting?
Aug 2001 (full month: 4138 granules)	Terra and Aqua	
7 Jul 2002 (full day: 132 granules)	Aqua	Quebec Smoke in NE US
8 Jul 2002 (full day: 136 granules)	Aqua	Quebec Smoke in NE US
6 Mar 2004 (full day: 132 granules)	Aqua	Asian Dust
7 Mar 2004 (full day: 138 granules)	Aqua	Asian Dust
Eight days in 2003 (full days: 1070 granules)	Aqua	Yearly Cycle
14 Nov 2005 (full day: 138 granules)	Terra	Low AOD globally
22 Apr 2001 (full day: 136 granules)	Terra	ACE-Asia
26 Jun 2002 (full day: 138 granules)	Terra	Summer time haze
Test_bed_Aqua: (39 granules)	Aqua	Test bed of interesting Aqua data
Test_bed_Terra: (102 granules)	Terra	Test bed of interesting Terra data

[a]Total granules = 6299.

141 individual granules that are known as the MODIS "test_bed." These granules include observations from both Terra and Aqua and are seasonally and yearly representative of the MODIS time series. For comparison, we ran V5.1 on the same set of granules. Note that the database used to derive the land surface relationships (350,000 Aqua and Terra data from 2000 to 2004) has a small overlap with our 6300 granule test bed. In that way, the comparison to AERONET shown in this section is not entirely independent of the formulation database. However, the data used in this section includes all values of τ and α, while the formulation data base was limited to specific ranges of these variables. Also, the data used here represent a comparison of spatiotemporal statistics, while in the formulation data base only the individual match between Sun photometer location and satellite overpass were used. Thus the plots shown here, while not entirely independent, offer a test of the new retrieval in more general conditions than in the specific formulation data. Figures 10 and 11 plot the comparisons of both V5.1 and V5.2 with the AERONET data, via the spatiotemporal colocation method of *Ichoku et al.* [2002].

[76] Figure 10 plots the retrieved MODIS τ against AERONET τ, both at 0.55 μm. The data have been sorted by AERONET τ and averaged into bins with equal numbers of observations in each bin. The mean and standard deviation of each bin are calculated and plotted in Figure 10 as a

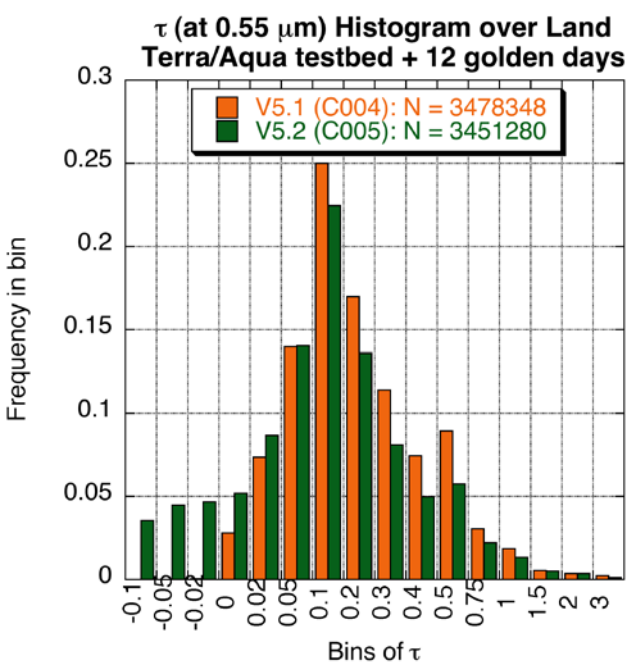

Figure 9. Histogram of retrieved τ (AOD) over land, from V5.2 (C005) in green, compared to V5.1 (C004) in orange. The data include the 141 granules of the Terra and Aqua "test_bed" as well as 12 complete days. The value of each bin refers to the minimum value of the bin (the max value would be the value of the next bin). Note that the general lognormal nature of the retrievals is preserved, except now there are some negative values.

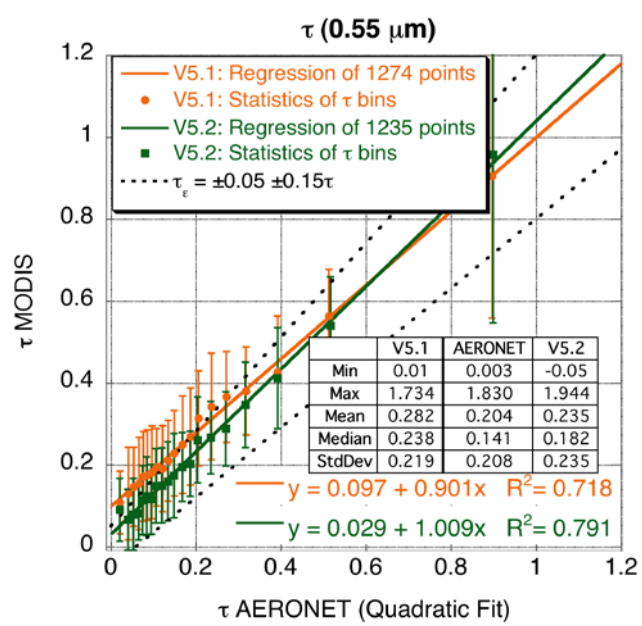

Figure 10. MODIS τ over land retrieved at 0.55 μm, compared with AERONET τ interpolated to 0.55 μm. The solid shapes and error bars represent the mean and standard deviation of the MODIS retrievals, in 20 bins of AERONET-derived τ. Both the retrievals from V5.1 (orange) and V5.2 (green) are shown. The regressions (solid lines) are for the cloud of all points before binning (not shown). The expected errors for MODIS (±0.05 $\pm0.15\tau$) are also shown (dashed lines).

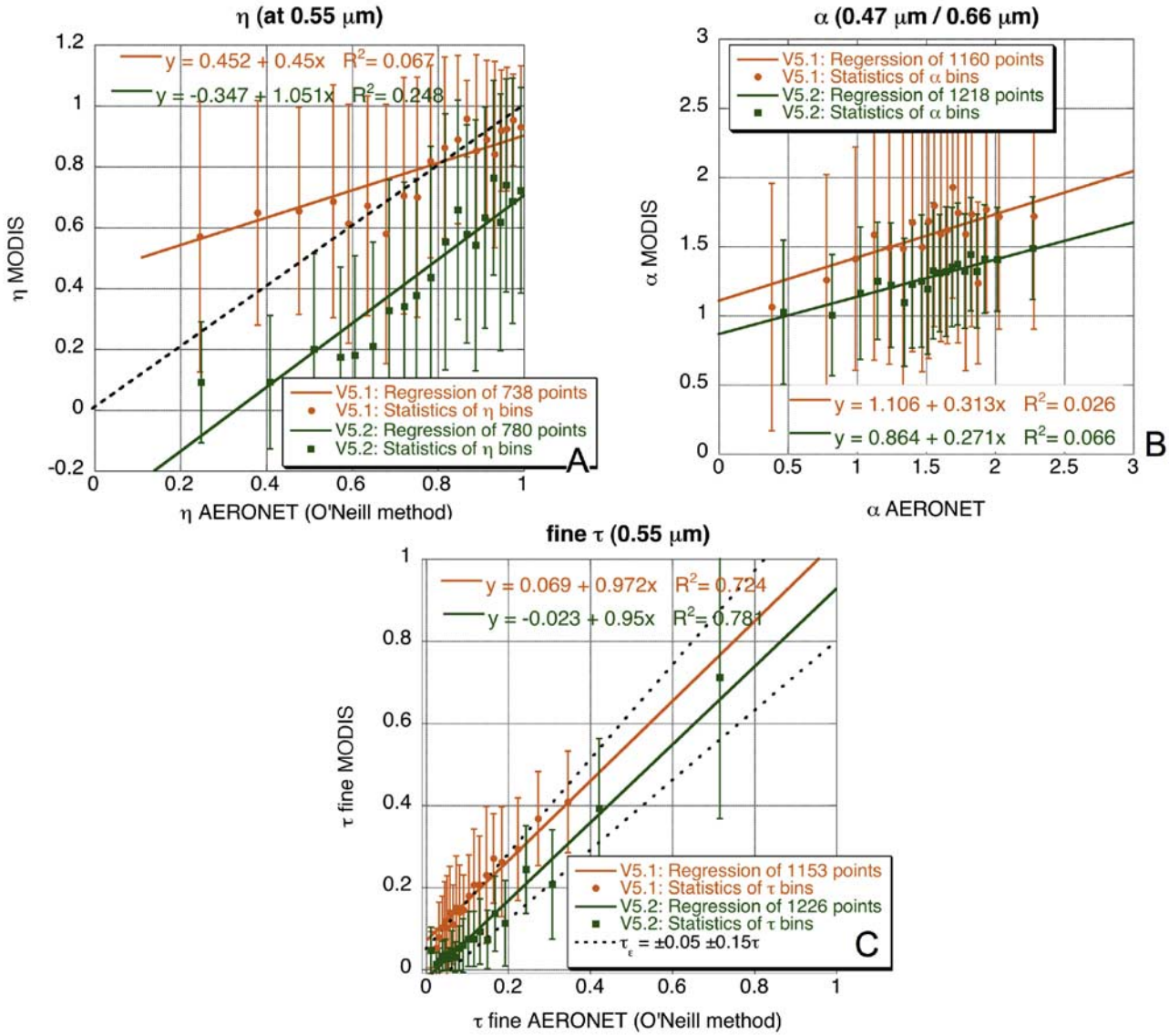

Figure 11. MODIS aerosol size retrievals compared with AERONET derived products. The solid shapes and error bars represent the mean and standard deviation of the MODIS retrievals, in 20 bins of AERONET-derived product. Both the retrievals from V5.1 (orange) and V5.2 (green) are shown. The regressions (solid lines) are for the cloud of all points (not shown). (a) The η over land retrieved at 0.55 μm, compared with AERONET η retrieved by the *O'Neill et al.* [2003] method. Note that η is defined differently for MODIS and AERONET and that we only show results for $\tau > 0.20$. (b) MODIS-derived α (0.466/0.644 μm) over land with AERONET α interpolated to the same wavelengths. (c) MODIS Fine τ over land retrieved at 0.55 μm, compared with AERONET Fine τ interpolated to 0.55 μm by quadratic fitting and the O'Neill method. The expected errors for MODIS ($\pm 0.05 \pm 0.15\tau$) are also shown (dashed lines).

solid dot and error bars. The correlation is calculated from the freely plotted points before binning, although the cloud of points is not shown in the plot. The regression equation has improved tremendously, from "y = 0.097 + 0.91x" to "y = 0.029 + 1.01x." Correlation R is also improved, from R = 0.847 to R = 0.894. It should be noted that slight differences in the number of points arise due to different selection of valid dark pixels and allowance of below zero τ retrievals.

[77] Figure 11a plots MODIS η against AERONET η, where AERONET η is calculated from Sun observations of spectral τ as described by *O'Neill et al.* [2003]. Keep in mind that unlike MODIS/AERONET comparisons of τ, MODIS and AERONET do not retrieve the same quantity labeled as η. The AERONET retrieval assumes one fine mode and one coarse mode. Thus AERONET η is the weighting between modes. The MODIS land η is a weighting between bimodal models, where fine-dominated models also contain a coarse mode and vice versa. The improvement to the MODIS η product is mainly its correlation to AERONET. Note that η is defined only when $\tau > 0.2$. Figures 11b and 11c show comparisons for derived prod-

ucts, including the Ångstrom Exponent (defined by 0.47 and 0.66 μm), and fine optical depth (i.e., $\tau^{f} = \tau \times \eta$), respectively. For fine τ, the correlation and slopes are nearly unchanged between V5.1 and V5.2; however, the offset decreases from +0.051 to −0.031. The result is that nearly two-thirds of all V5.2 MODIS Fine τ fall within expected errors defined by equation (2). Note again that the difference in the number of points is due to different selection of dark pixels and treatment of negative τ retrievals. The Ångstrom exponent has little improvement from V5.1 to V5.2, except for slightly better but still poor correlation with the AERONET measured quantities. In general, the changes to the MODIS aerosol retrieval algorithm described here have resulted in a much less biased τ and τ^{f} products than the previous algorithm. MODIS η and other size parameters correlate better with AERONET, although it still leaves room for improvement.

8. Conclusion

[78] In this document, we have introduced a second-generation operational algorithm for deriving aerosol optical properties over dark land surfaces, from MODIS observed spectral reflectance. In the new algorithm, we have updated a number of assumptions, including the VISvs2.12 surface reflectance parameterization, and the statistical implications of deriving below zero aerosol optical thickness. Most significantly, instead of an independent two-channel retrieval, this new algorithm performs a simultaneous three-channel inversion to make use of aerosol information contained in the SWIR (2.12 μm) channel. We have coupled these changes with updated representative global aerosol optical models and lookup tables.

[79] This algorithm has been tested both for its theoretical ability to derive aerosol properties and on a test bed of 6300 MODIS granules. Compared with colocated AERONET sites, the new MODIS algorithm retrieves aerosol properties more accurately than the previous. Specifically, the retrievals of total τ meet expected accuracy levels ($\pm 0.05 \pm 0.15\ \tau$). MODIS/AERONET τ regression has an equation of: y = 1.01x + 0.03, R = 0.90. Global (the 6300 granules) mean τ has been reduced from 0.28 to 0.21. Retrievals of η show less significant improvement, but are still better correlated with AERONET results than previous versions. Retrievals of spectral Ångstrom Exponent show little or no improvement at this time. However, the new algorithm's derivation of fine τ ($\tau \times \eta$) is much improved. This product may be related to the anthropogenic contribution to the total τ [e.g., *Kaufman et al.*, 2005] and has specific applications for the climate community. Finally, the C005 products' quality assurance (QA) has been overhauled and is now more useful to users within the aerosol community.

[80] **Acknowledgments.** We are grateful to Charles Ichoku for providing us with the MAPSS code and sound advice, to Tom Eck and the AERONET team for their data and advice, to Mian Chin and Pete Colarco for evaluating the sanity of our products (and advice), and to Alexander Ignatov who advised us that negatives retrievals were meaningful. This work was greatly improved by the thoughtful and detailed comments from our anonymous reviewers and MODIS users around the world.

References

Ahmad, Z., and R. S. Fraser (1982), An iterative radiative transfer code for ocean-atmosphere system, *J. Atmos. Sci.*, *39*, 656–665.

Al-Saadi, J., et al. (2005), Improving national air quality forecasts with satellite aerosol observations, *Bull. Am. Meteorol. Soc.*, *86*(9), 1249–1261.

Anderson, T. L., Y. Wu, D. A. Chu, B. Schmid, J. Redemann, and O. Dubovik (2006), Testing the MODIS satellite retrieval of aerosol fine-mode fraction, *J. Geophys. Res.*, *110*, D18204, doi:10.1029/2005JD005978.

Bodhaine, B. A., et al. (1999), On Rayleigh optical depth calculations, *J. Atmos. Ocean. Technol.*, *16*(11), 1854–1861.

Chu, D. A., et al. (2002), Validation of MODIS aerosol optical depth retrieval over land, *Geophys. Res. Lett.*, *29*(12), 8007, doi:10.1029/2001GL013205.

Chu, D. A., Y. J. Kaufman, G. Zibordi, J. D. Chern, J. Mao, C. Li, and B. N. Holben (2003), Global monitoring of air pollution over land from EOS-Terra MODIS, *J. Geophys. Res.*, *108*(D21), 4661, doi:10.1029/2002JD003179.

Chu, D. A., et al. (2005), Evaluation of aerosol properties over ocean from Moderate Resolution Imaging Spectroradiometer (MODIS) during ACE-Asia, *J. Geophys. Res.*, *110*, D07308, doi:10.1029/2004JD005208.

Dave, J. V. (1970), Intensity and polarization of radiation emerging from a plane-parallel atmosphere containing monodispersed aerosols, *Appl. Opt.*, *9*(12), 2673–2684.

Dubovik, O., and M. D. King (2000), A flexible inversion algorithm for retrieval of aerosol optical properties from Sun and sky radiance measurements, *J. Geophys. Res*, *105*(D16), 20,673–20,696.

Dubovik, O., et al. (2002), Non-spherical aerosol retrieval method employing light scattering by spheroids, *Geophys. Res. Lett.*, *29*(10), 1415, doi:10.1029/2001GL014506.

Dubovik, O., et al. (2006), Application of light scattering by spheroids for accounting for particle nonsphericity in remote sensing of desert dust, *J. Geophys. Res.*, *111*, D11208, doi:10.1029/2005JD006619.

Dutton, E. G., P. Reddy, S. Ryan, and J. J. DeLuisi (1994), Features and effects of aerosol optical depth observed at Mauna Loa, Hawaii: 1982–1992, *J. Geophys. Res.*, *99*, 8295–8306.

Eck, T. F., et al. (1999), Wavelength dependence of the optical depth of biomass burning, urban, and desert dust aerosols, *J. Geophys. Res*, *104*(D24), 31,333–31,349.

Evans, K. F., and G. L. Stephens (1991), A new polarized atmospheric radiative transfer model, *J. Quant. Spectrosc. Radiat. Transfer*, *46*(5), 413–423.

Fraser, R. H., R. A. Ferrare, Y. J. Kaufman, and S. Mattoo (1989), Algorithm for atmospheric corrections of aircraft and satellite imagery, *Tech. Memo. 100751*, NASA Goddard Space Flight Cent., Greenbelt, Md.

Gatebe, C. K., et al. (2001), Sensitivity of off-nadir zenith angles to correlation between visible and near-infrared reflectance for use in remote sensing of aerosol over land, *IEEE Trans. Geosci. Remote Sens.*, *39*(4), 805–819.

Holben, B. N., et al. (1998), AERONET - A federated instrument network and data archive for aerosol characterization, *Remote Sens. Environ.*, *66*(1), 1–16.

Ichoku, C., et al. (2002), A spatio-temporal approach for global validation and analysis of MODIS aerosol products, *Geophys. Res. Lett.*, *29*(12), 8006, doi:10.1029/2001GL013206.

Intergovernmental Panel on Climate Change (2001), *Climate Change 2001: The Scientific Basis*, edited by J. T. Houghton et al., 944 pp., Cambridge Univ. Press, Cambridge, UK.

Karnieli, A., Y. J. Kaufman, L. A. Remer, and A. Wald (2001), AFRI-aerosol free vegetation index, *Remote Sens. Environ.*, *77*(1), 1–21.

Kaufman, Y. J., and C. Sendra (1988), Algorithm for atmospheric corrections of visible and Near IR satellite imagery, *Int. J. Remote Sens.*, *9*, 1357–1381.

Kaufman, Y. J., et al. (1997a), Operational remote sensing of tropospheric aerosol over land from EOS moderate resolution imaging spectroradiometer, *J. Geophys. Res*, *102*(D14), 17,051–17,067.

Kaufman, Y. J., et al. (1997b), The MODIS 2.1-μm channel - Correlation with visible reflectance for use in remote sensing of aerosol, *IEEE Trans. Geosci. Remote Sens.*, *35*(5), 1286–1298.

Kaufman, Y. J., et al. (2002), Relationship between surface reflectance in the visible and mid-IR used in MODIS aerosol algorithm: Theory, *Geophys. Res. Lett.*, *29*(23), 2116, doi:10.1029/2001GL014492.

Kaufman, Y. J., et al. (2005), Aerosol anthropogenic component estimated from satellite data, *Geophys. Res. Lett.*, *32*, L17804, doi:10.1029/2005GL023125.

King, M. D., W. P. Menzel, Y. J. Kaufman, D. Tanre, B.-C. Gao, S. Platnick, S. A. Ackerman, L. A. Remer, R. Pincus, and P. A. Hubanks (2003), Cloud and aerosol properties, precipitable water, and profiles of temperature and humidity from MODIS, *IEEE Trans. Geosci. Remote Sens.*, *41*, 442–458.

Kleidman, R. G., et al. (2005), Comparison of moderate resolution Imaging spectroradiometer (MODIS) and aerosol robotic network (AERONET) remote-sensing retrievals of aerosol fine mode fraction over ocean, *J. Geophys. Res.*, *110*, D22205, doi:10.1029/2005JD005760.

Levy, R. C., et al. (2004), Effects of neglecting polarization on the MODIS aerosol retrieval over land, *IEEE Trans. Geosci. Remote Sens.*, *42*(11), 2576–2583.

Levy, R. C., et al. (2005), Evaluation of the MODIS aerosol retrievals over ocean and land during CLAMS, *J. Atmos. Sci.*, *62*(4), 974–992.

Levy, R. C., et al. (2007), Global aerosol optical properties and application to MODIS aerosol retrieval over land, *J. Geophys. Res.*, *112*, D13210, doi:10.1029/2006JD007815.

Li, R. R., et al. (2005), Snow and ice mask for the MODIS aerosol products, *IEEE Geosci. Remote Sens. Lett.*, *2*(3), 306–310.

Lyapustin, A. I. (2001), Three-dimensional effects in the remote sensing of surface albedo, *IEEE Trans. Geosci. Remote Sens.*, *39*(2), 254–263.

Martins, J. V., et al. (2002), MODIS Cloud screening for remote sensing of aerosols over oceans using spatial variability, *Geophys. Res. Lett.*, *29*(12), 8009, doi:10.1029/2001GL013252.

Moody, E. G., M. D. King, S. Platnick, C. B. Schaaf, and F. Gao (2005), Spatially complete global spectral surface albedos: Value-added datasets derived from Terra MODIS land products, *IEEE Trans. Geosci. Remote Sens.*, *43*, 144–158.

O'Neill, N. T., T. F. Eck, A. Smirnov, B. N. Holben, and S. Thulasiraman (2003), Spectral discrimination of coarse and fine mode optical depth, *J. Geophys. Res.*, *108*(DX), 4559, doi:10.1029/2002JD002975.

Remer, L. A., et al. (2001), Angular and seasonal variation of spectral surface reflectance ratios: Implications for the remote sensing of aerosol over land, *IEEE Trans. Geosci. Remote Sens.*, *39*(2), 275–283.

Remer, L. A., et al. (2005), The MODIS aerosol algorithm, products, and validation, *J. Atmos. Sci.*, *62*(4), 947–973.

Tanré, D., M. Hermon, and Y. J. Kaufman (1996), Information on aerosol size distribution contained in solar reflectance spectral radiances, *J. Geophys. Res.*, *101*(D14), 19,043–19,060.

Tanré, D., et al. (1997), Remote sensing of aerosol properties over oceans using the MODIS/EOS spectral radiances, *J. Geophys. Res.*, *102*(D14), 16,971–16,988.

U.S. Government Printing Office (1976), *U.S. Standard Atmosphere*, Washington, D. C.

Vermote, E. F., et al. (1997), Second simulation of the satellite signal in the solar spectrum, 6S: An overview, *IEEE Trans. Geosci. Remote Sens.*, *35*(3), 675–686.

Wiscombe, W. J. (1981), Improved Mie scattering algorithms, *Appl. Opt.*, *19*, 1505–1509.

Yu, H., et al. (2006), A review of measurement-based assessments of aerosol direct radiative effect and forcing, *Atmos. Chem. Phys.*, *6*, 613–666.

Y. J. Kaufman and L. A. Remer, Laboratory for Atmospheres, NASA Goddard Space Flight Center, Code 613.2, Greenbelt, MD 20771, USA.

R. C. Levy and S. Mattoo, Science Systems and Applications Inc., 10210 Greenbelt Road, Suite 600, Lanham, MD 20706, USA. (levy@climate.gsfc.nasa.gov)

E. F. Vermote, Department of Geography, University of Maryland, 209 Hartwick, College Park, MD 20742, USA.